PHYSICAL AND CHEMICAL PROPERTIES OF BIMETALLIC DOPED VANADIUM PHOSPHORUS OXIDE CATALYSTS

PRAKAS A/L PALANYCHAMY

UNIVERSITI TUNKU ABDUL RAHMAN

PHYSICAL, CHEMICAL AND REACTIVITY PROPERTIES OF BISMUTH-BARIUM BIMETALLIC DOPED VANADIUM PHOSPHORUS OXIDE CATALYSTS

PRAKAS A/L PALANYCHAMY

A project report submitted in partial fulfilment of the requirements for the award of Bachelor of Engineering (HONS) Chemical Engineering

Faculty of Engineering and Science
Universiti Tunku Abdul Rahman

May 2012

DECLARATION

I hereby declare that this project is based on my original work except for citations and quotations which have been duly acknowledged. I also declare that it has not been previously or concurrently submitted for any other degree or award at UTAR or other institutions.

Signature : _____

Name : Prakas a/l Palanychamy

ID. No : 08 UEB 04520

Date : 11th May 2012

APPROVAL FOR SUBMISSION

I certify that this project entitled "**PHYSICAL AND CHEMICAL PROPERTIES OF BIMETALLIC DOPED VANADIUM PHOSPHORUS OXIDE CATALYSTS**" was prepared by **PRAKAS A/L PALANYCHAMY** has met the required standard for submission in partial fulfilment of the requirements for the award of Bachelor of Engineering (HONS) Chemical Engineering at Universiti Tunku Abdul Rahman.

Approved by,

Signature : _____

Supervisor : Dr. Leong Loong Kong

Date : 11th May 2012

The copyright of this report belongs to the author under the terms of copyright Act 1987 as qualified by Intellectual Property Policy of Universiti Tunku Abdul Rahman. Due acknowledgement shall always be made of the use of any material contained in, or derived from, this report.

© 2012, Prakas a/l Palanychamy. All right reserved.

Specially dedicated to my beloved father, mother and younger sister.

ACKNOWLEDGEMENTS

I would like to thank everyone who had contributed to the successful completion of this project. I would like to express my gratitude to my research supervisor, Dr. Leong Loong Kong for his invaluable advice, guidance and enormous patience throughout the development of the research. His guidance helped me from scratch till the completion of this project, and hence it was a vital factor towards the completion of this project.

In addition, I would to sincerely thank the lab officer Miss Zoey Kang and Dr. Leong's master students Max and Matthew for providing more than enough assistance in carrying out this research, from the synthesis stage till the end of the thesis writing. Without their guidance and knowledge, this research would have not come to a completion.

Moreover, I would also like to thank Cik Azlyana binti Ismail, who is my moderator for this project. She had pin pointed my mistakes, both in my reports and presentations which led to me to further improve my thesis quality.

Also not forgetting to thank my teammates for their wisdom and help they offered to me to complete this research. In addition I would like to express my gratitude to my loving parent and younger sister who had encouraged and assisted me financially throughout the completion of my degree and research.

PHYSICAL AND CHEMICAL PROPERTIES OF BIMETALLIC DOPED VANADIUM PHOSPHORUS OXIDE CATALYSTS

ABSTRACT

A series of vanadyl pyrophosphate, $(VO)_2P_2O_7$, catalyst prepared via the sesquihydrate route was doped with Ba 5 % and a series of 1 %, 3 % and 5 % of Bi dopant and calcined in a reaction flow of 0.75 % *n*-butane in air mixture at 733 K for 6 h. The dihydrate precursor was synthesized by refluxing it with 1-butanol for 6 h. The catalyst were denoted as VPOs-Ba5; VPOs-Ba5,Bi1; VPOs-Ba5,Bi3 and VPOs-Ba5,Bi5 respectively. The X-ray diffraction pattern for all the catalyst showed similar diffraction patterns with well crystallized $(VO)_2P_2O_7$ phase. SEM images showed that all the catalyst's surface morphologies were found to be in platelet like crystals, agglomerated as clusters. BET result surface area measurement showed that VPOs-Ba5,Bi1 had the highest surface area of 17.54 $m^2\ g^{-1}$, followed by 16.51 $m^2\ g^{-1}$, 15.13 $m^2\ g^{-1}$ and 12.69 $m^2\ g^{-1}$ for VPOs-Ba5,Bi3, VPOs-Ba5,Bi5 and VPOs-Ba5 respectively. From EDX analysis, it is known that the optimal catalyst composition is characterized by slight excess of phosphate with the average P/V ratio obtained for all the catalyst was in between 1.026 to 1.097. Redox titration result of more than 4.0 for all the samples shows that the samples consists of both V^{4+} and V^{5+} phases, with addition of bismuth increasing the V_{AV} favouring more to selectivity. Temperature programmed reduction (TPR) in H_2 profiles for all the catalyst gave three reduction peaks. Ratio for oxygen removal of V^{5+}/V^{4+} increased as the percentage of Bi addition was increased, with VPOs-Ba5,Bi1 having the most oxygen desorbed from the surface, as much as 4.701×10^{21} atom g^{-1}.

TABLE OF CONTENTS

LIST OF TABLES

LIST OF FIGURES

LIST OF SYMBOLS/ABBREVIATIONS

VPO	vanadium phosphorus oxide
V^{3+}	vanadium at oxidation state of +3
V^{4+}	vanadium at oxidation state of +4
V^{5+}	vanadium at oxidation state of +5
t	crystallite size for (h k l) phase, Å
$ß_{hkl}$	full width at half maximum (FWHM) at (h k l) peak, rad
θ_{hkl}	diffraction angle for (h k l) phase, °
λ	X-rays wavelength of radiation for CuKa, Å
V_1	volume of potassium permanganate used in first stage, cm^3
V_2	volume of ammonium iron (II) sulphate used in second stage, cm^3
V_3	volume of ammonium iron (II) sulphate used in third stage, cm^3
V^{3+}	concentration of vanadium at oxidation number of +3
V^{4+}	concentration of vanadium at oxidation number of +4
V^{5+}	concentration of vanadium at oxidation number of +5
V_{AV}	average oxidation number of vanadium (V_{AV})

LIST OF APPENDICES

CHAPTER 1

INTRODUCTION

1.1 Background of Catalysis

The catalytic power was discovered in early 19th century. Chemists and physicists noticed that a number of chemical reactions were affected by trace amounts of substances that were not consumed in the reaction. These includes traces of acid that causes hydrolysis of starch; low concentration of metal ions which improve the decomposition of hydrogen peroxide. Scientist J.W. Dobereiner, Michael Faraday and Peregrine Philips have contributed in this catalytic power discovery. Later in 1836, the first attempt to rationalize these findings was made by J.J. Berzelius (Bond, 1987).

Catalytic power actually means that substances are able to awake affinities which are asleep at a specific temperature by their mere presence and not by their own affinity. The catalyst concept was improved to an acceptable definition by the Greek's and Chinese's catalyst concept. The Greek's refers a catalyst as a substance that breaks down the normal forces which inhibit the reactions of the molecules. Chinese explains that the catalyst breaks down the barrier which is an essential prerequisite to bring the particles together (Bond, 1987).

The final acceptable definition of the catalyst is a chemical substance that accelerates the rate of a chemical reaction until approaching equilibrium, by lowering the activation energy for the reaction to take place and without being consumed in the reaction (Viswanathan et al., 2002).

1.2 Role of Catalysis

Catalysis is a phenomenon, in which a relatively small amount of a foreign material, called a catalyst, increases the rate of a chemical reaction. Interacting with the reactants the catalyst enters into the reaction cycle, but is regenerated in its last step and therefore is not consumed in its course, ideally remaining unchanged after its completion. Thus the amount of product obtained with the given amount of catalyst is theoretically unlimited, in practice usually very large (Haber, 1994).

The acceleration effect of a catalyst is achieved for a given reaction, through interaction with the substrates. A new reaction pathway, usually multistep, characterized by a lower energy barrier and an appropriate spatial arrangement of reactants facilitating to overcome the entropy barrier (Haber, 1994).

Catalysis is a key technology to achieve the objectives of sustainable (green) chemistry. After introducing the concepts of sustainable (green) chemistry and a brief assessment of new sustainable chemical technologies, the relationship between catalysis and sustainable (green) chemistry is discussed and illustrated via an analysis of some selected and relevant examples (Haber, 1994).

Emphasis is also given to the concept of catalytic technologies for scaling-down chemical processes, in order to develop sustainable production processes which reduce the impact on the environment to an acceptable level that allows self-depuration processes of the living environment (Haber, 1994).

1.3 Non-Catalysed Reaction

Maxwell-Boltzmann distribution (Figure 1.1) states the reactant molecules possess a wide range of energies at any temperature. For successful conversion of reactant to product, the reactant molecules must possess at least the activation enthalpy when they collide (Bond, 1987).

Lose of the kinetic energy occurs during the collision as work is done to break the bonds. Only particles with enough kinetic energy or more than the activation energy will react. Once the activation enthalpy is low, higher amount of the reactant molecules are able to overcome the activation energy. The collision will lead to the conversion of the reactant into products (Bond, 1987).

Only a few reactant molecules will have enough energy if the activation energy is high. Therefore, only a few collisions will result in a successful reaction and the rate of conversion of product will be slow (Bond, 1987).

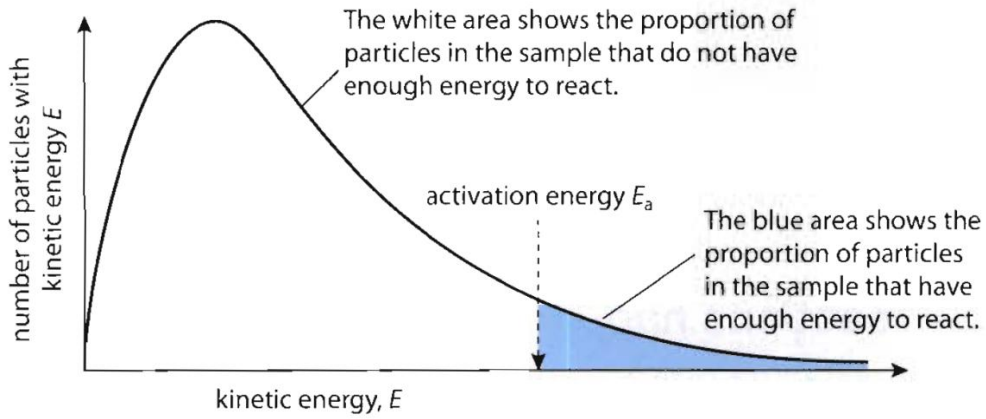

Figure 1.1: Maxwell-Boltzmann Distribution

1.4 Catalyst in Reaction

Catalyst provides an alternative path involving a different transition state with lower activation energy. Catalysts can increase the rate of a reaction which is only thermodynamically feasible, but cannot initiate a reaction which is thermodynamically unfavourable (Bond, 1987).

The position of the equilibrium attained remains unchanged, with the presence of the catalyst since the rate of the forward and reverse reactions are equally affected. Thermodynamic law states there is no existing situation with two different equilibrium positions. However, the change of two different free energies could coexist, where the difference between the initial and final states with or without the usage of a catalyst that causes the change (Bond, 1987).

Figure 1.2 shows that the uncatalyzed reaction (red line) requires higher activation energy than a catalysed reaction (green line). Also noted is that both the uncatalyzed and catalysed reaction exhibits an identical free energy change.

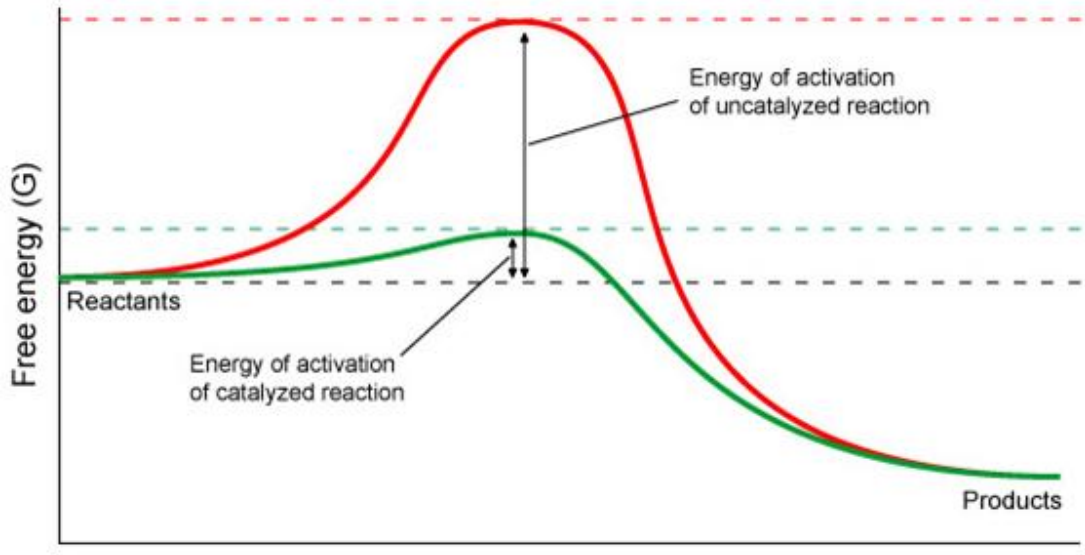

Figure 1.2: Comparison between Catalysed and Uncatalyzed Reaction

1.5 Requirements of a Catalyst

Catalyst would affect the overall cost of the manufacturing process in the industry sectors and hence it needed to be given great considerations. For a commercial catalyst, it must possess several desirable features such as high selectivity and high activity per unit volume of the reactor (Felthouse et al., 2001).

High selectivity reduces the cost of separating the products from those unwanted or waste compounds as only a small fraction of the reactant turn into products. As for a catalyst having high activity per unit volume of the reactor, it can reduce the cost of the catalyst per unit of product produced (Felthouse et al., 2001).

Compared to the pellet size, porous supports are more often used even though it is accounted that diffusion and mass transport will be lower inside the support rather than in the bulk solution (Felthouse et al., 2001).

Catalyst also need to be mechanically strong and stable at desired temperatures for the reaction to be carried out. Finally, a good catalyst must be chemically inert to the reactants, products and the solvents used in a particular reaction (Felthouse et al., 2001).

1.6 Types of Catalyst

Catalyst can be classfied into many different categories according to their properties such as state of segregation, composition and molecular structure. Most commonly used method is the state of segregation which is the way catalyst react with the reactants. Generally there are three groups of catalysts namely: heterogeneous catalyst, homogeneous catalyst and biocatalyst.

1.6.1 Heterogeneous Catalyst

Heterogeneous catalysis is distinguished from the homogeneous catalysis by the different phases present in a chemical reaction. Heterogeneous catalysis takes place between several phases where the catalyst usually is a solid and the reactants are either in gaseous or liquid phase (Chorkendorff & Niemantsverdriet, 2003).

Solid catalyst which are non porous are impenetrable. This type of catalytic reactions occurs where the reactants absorb onto the surface of a solid catalyst. The reactants are activated by chemical interaction with the catalyst surface and transformed into products. Products detach themselves form the catalyst surface and the catalyst is ready for the next reaction (Viswanathan et al., 2002).

As an introductory example we take one of the key reactions in cleaning automotive exhaust, the catalytic oxidation of CO on the surface of noble metals such as platinum, palladium and rhodium. To describe the process, we will assume that the metal surface consists of active sites, denoted as "*e**".

The catalytic reaction cycle begins with the adsorption of CO and O_2 on the surface of platinum, whereby the O_2 molecule dissociates into two O atoms (*e** indicates that the atom or molecule is adsorbed on the surface, i.e. bound to the site *):

$$O_2 + 2e^* \leftrightarrow 2O^* \quad (1.1)$$

$$CO + e^* \leftrightarrow CO^* \quad (1.2)$$

The adsorbed O atom and the adsorbed CO molecule then react on the surface to form CO_2, which, being very stable and relatively unreactive and interacts only weakly with the platinum surface and desorbs almost instantaneously:

$$CO^* + O^* \leftrightarrow CO_2 + 2e^* \quad (1.3)$$

1.6.2 Homogeneous Catalyst

A homogeneous catalyst is molecularly dispersed in the reactants, which are most commonly in liquid state. Catalysis of the transformation of organic molecules by acids or bases represents one of the most widespread types of homogeneous catalysis. In addition, the catalysis of organic reactions by metal complexes in solution has grown rapidly in both scientific and industrial importance (Bond, 1987).

One of the most common examples is the decomposition of ozone in the atmosphere via a reaction with chlorine atoms:

$$Cl + O_3 \rightarrow ClO_3 \quad (1.4)$$

$$ClO_3 \rightarrow ClO + O_2 \quad (1.5)$$

$$ClO + O \rightarrow Cl + O_2 \quad (1.6)$$

Cl atom acts as a catalyst to accelerate the reaction and leaves the reaction cycle unaltered after the reaction. Since both the reactants are in the same gas phase, this reaction is an example of homogeneous catalysis (Chorkendorff & Niemantsverdriet, 2003).

1.6.3 Biocatalyst

Enzymes are nature's catalysts. For the moment it is sufficient to consider an enzyme as a large protein, the structure of which results in a very shape-specific active site (Figure 1.3). Having shapes that are optimally suited to guide reactant molecules (usually referred to as substrates) in the optimum configuration for reaction, enzymes are highly specific and efficient catalysts.

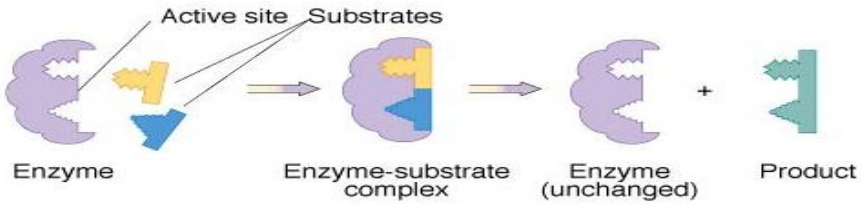

Figure 1.3: Representation of Shape Specific Active Sites

1.7 Problem Statement

Maleic anhydride is a versatile chemical intermediate used to make unsaturated polyester resins, lube oil additives, alkyd resins, and a variety of other products. In 1995, global production of maleic anhydride was estimated at 1.8 billion pounds, with an estimated value of $700 million.

Over the years, world consumption has increased at an average annual rate of 5.8 %, with the fastest growth occurring in Asia, where it is used as an intermediate for production of 1,4-butanediol (Baylis, 1996).

The goal of this project is to design a grass roots facility that is capable of producing 40 million pounds of maleic anhydride per year from *n*-butane. However, the complexity of the reaction as well as limited knowledge on the selective oxidation of *n*-butane had raised concerns on the feasibility of the project.

To date, the optimum selectivity and activity for VPO catalyst in the production of maleic anhydride, MA is still in extensive studies. Based on the production information from BASF Petronas (2010), the maximum conversion (activity) of VPO catalyst attempted was at 82 % with 65 % selectivity. Even though an acceptable amount of MA is obtained, a higher selectivity catalyst would lower the by products produced.

Further research is being conducted to improve both the selectivity and activity of the catalyst to more than 90 %. However, when such a dramatic improvement is desired, there are repercussions; in this case the cost of the catalyst is will be higher. Thus, costing should always be in mind along with desired selectivity and activity to ensure an optimal and cost effective catalyst is produced.

Thus, it is important to have an insight on the characterization and catalytic properties of the catalyst used in the selective oxidation of *n*-butane to maleic anhydride. Two most important aspects of a catalyst considered here would be its activity and selectivity towards maleic anhydride (Baylis, 1996).

1.8 Objectives of Research

The main objectives of this research is to have a deeper understanding of the characterization and catalytic properties of the synthesized VPOs catalysts. Besides that, this research is also to study the effect of dopant addition to the VPOs catalysts.

CHAPTER 2

LITERATURE REVIEW

2.1 Maleic Anhydride

Maleic anhydride is a versatile molecule that lends itself to many applications requiring a number of properties and functionalities. With three active sites (two carboxyl groups and one double bond), it is an excellent joining and cross linking agent (Figure 2.1). Its major end use, representing well over half of global demand is in the manufacture of unsaturated polyester resins, where it's cross linking abilities are important (Maleic Anhydride, 2009).

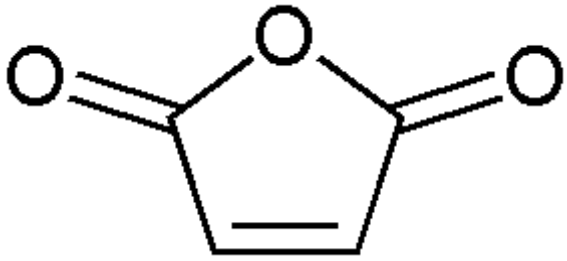

Figure 2.1: Molecular Structure of Maleic Anhydride

It is an important intermediate in the fine chemical industry, particularly in the manufacture of agricultural chemicals and lubricating oil additives. It is also a component of several copolymers in the engineering polymers sectors (Maleic Anhydride, 2009).

Maleic anhydride is the classic Diels-Alder reagent. For the research carried out in 1928 on the reaction between maleic anhydride and 1,4-butadiene, Diels and Alder were awarded the Nobel prize.. It is through this reaction that maleic anhydride was used in many pesticides and pharmaceuticals applications (Maleic Anhydride, 2009).

It is also an environmentally acceptable molecule, which is an important added bonus in its applications. Some examples of the special chemicals that can be prepared from maleic anhydride include tartaric acid, diethyl and dimethyl succinate, and malic acid. The physical properties of maleic anhydride are tabulated in Table 2.1 (Maleic Anhydride, 2009).

Table 2.1: Physical Properties of Maleic Anhydride

Properties	Maleic Anhydride
Formula	$C_4H_2O_3$
Molecular weight	98.06
Melting Point (°C)	52.85
Boiling Point (°C)	202
Heat of Formation (kJ/mol)	-470.41
Heat of Combustion (kJ/mol)	-1389.5
Heat of Vaporization (kJ/mol)	54.8
Crystalline Form	Orthorhombic

2.2 Production of Maleic Anhydride

In the early 1930's benzene was the primary raw material used in the production of maleic anhydride. The production by the vapour phase oxidation of benzene was dominant around 1980's. It was determined later on that benzene was an inefficient feedstock in the production of maleic anhydride due to the excess of two carbon atoms in the starting material. It was first prepared in the 1830's but was commercially manufactured only a century later (Felthouse et al., 2001).

From the molecular formula for maleic anhydride, ($C_4H_2O_3$) we know that the production of maleic anhydride only needs four carbons. Thus, the earlier raw material benzene was substituted by *n*-butane. No carbon lost in the production of maleic anhydride, lower price, higher availability in many regions, safe compound without any harm to health, non-hazardous and lower flammability limits are the primary advantages of *n*-butane compared to benzene. These factors led to the production of maleic anhydride using *n*-butane at Monsanto's J.F Queeny plant in 1974 (Felthouse et al., 2001).

Daxiang Wang and co-workers reported that selective oxidation of butane to maleic anhydride (MA) on vanadyl pyrophosphate (VPO) catalyst based on Mars-van Krevelen Mechanism. In commercialized process of producing maleic anhydride, circulating fluidized bed riser reactors are used where the reduction and re-oxidation steps of the VPO catalyst are spatially separated into two separate reactors. It behaves differently under transient condition because the VPOs catalyst surface structure is very sensitive to the gas phase composition (Wang, 2002).

Huang and co-workers concluded that the re-oxidation of the catalyst in the two bed process for maleic anhydride from *n*-butane should be carried out at a higher temperature than the butane partial oxidation step. In the case of VPOs catalysis, this temperature should be between 500ºC and 620ºC. However, cyclic experiments shows that when the two steps are carried out at temperature range between 416ºC and 580ºC, a significant improvement in butane conversion, selectivity and yield to maleic anhydride is observed (Huang et al., 2002).

2.3 Benzene Oxidation

For 50 years, the main process route to maleic anhydride was the oxidation of benzene in the vapour phase, and it remains a commercial route outside the United States accounting for around 15 % to 20 % of global capacity (Maleic Anhydride, 2009).

Relatively high benzene costs are making the process obsolescent, but it will be continuously used by companies with no alternative feedstock. The technology is very similar to fixed bed processes using *n*-butane. Thus, many fixed bed benzene plants have been retrofitted to use *n*-butane (Maleic Anhydride, 2009).

The oxidation process can be divided into two steps, the reaction and recovery. The reaction step is a typical process using benzene as a feedstock passing a preheated vapour mixture of air and benzene over a catalyst disposed in reactor. The principal reaction of the process can be represented by the chemical equation below (Figure 2.2), although it should be noted that the ratio of CO to CO_2 is not fixed (Maleic Anhydride, 2009).

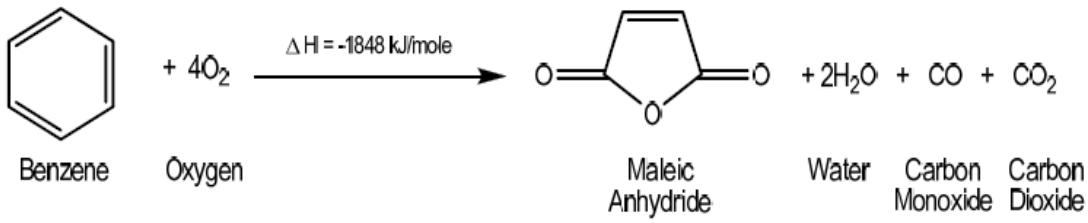

Figure 2.2: Benzene Oxidation

The catalyst used consists of supported vanadium oxide. Those supports are an inert oxide such as kisselguhr alumina or silica with low surface area because it could adversely affect the conversion of benzene to maleic anhydride if it has high surface area (Trivedi & Cullbertson, 1982)

2.4 *n*-Butane Oxidation

The first commercial process which used the *n*-butane as a feedstock was started in 1974 by Monsanto. This reaction of *n*-butane to maleic anhydride is a 14 electrons oxidation which occurs on the catalyst surface. In this 14 electrons oxidation reaction, eight hydrogen atoms abstracted, three oxygen atoms inserted and a ring closure is performed (Felthouse et al., 2001).

The partial oxidation of *n*-butane is very exothermic. Figure 2.3 shows the chemical reaction and the energy released from *n*-butane oxidation which exceeds that of benzene and this is reflected in the steam co-products (Maleic Anhydride, 2009).

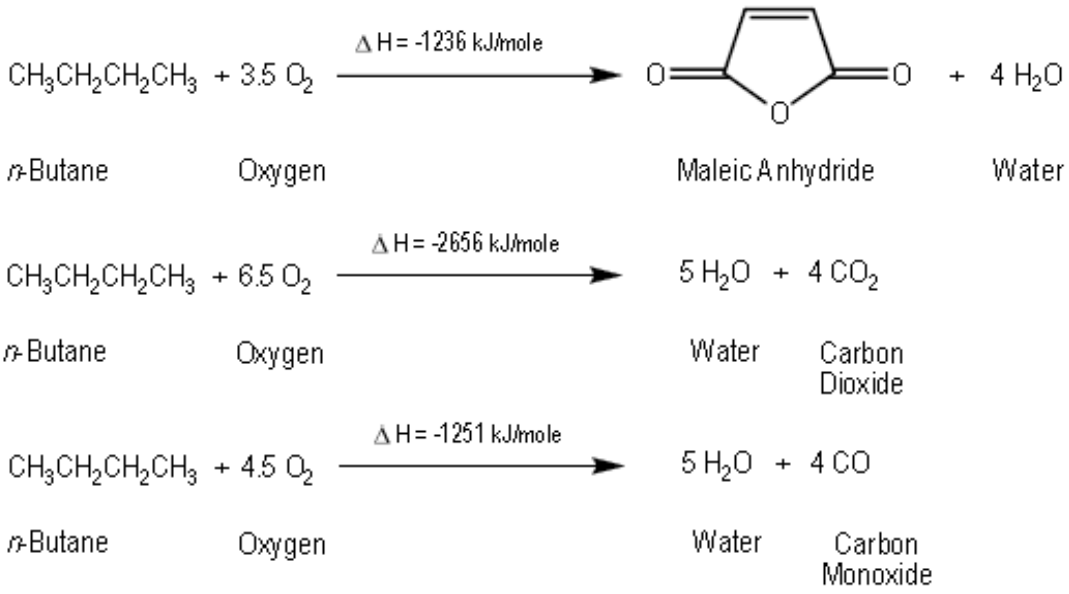

Figure 2.3: *n*-Butane Oxidation

Butane based catalyst technology consist of three technologies, namely Butane Based Fixed-Bed Process Technology, Fluidized-Bed Process Technology and Transport-Bed Process Technology. Each of these technologies differs from one another due to the reactor used to carry out the process (Felthouse et al., 2001).

2.5 Process of oxidizing *n*-Butane to Maleic Anhydride

In the conversion of *n*-butane to maleic anhydride, the *n*-butane in gas form flow through the vanadyl pyrophosphate, $(VO)_2P_2O_7$ catalyst at a temperature of 460ºC and a duration around 6 hours. As the *n*-butane flows through the catalyst, the gas will absorb on the catalyst's surface, where the chemical reaction occurs. The oxygen atom from the catalyst will be removed by *n*-butane and forms a complex. When this complex desorbs from the catalyst, the final desired product, maleic anhydride is formed. Summary of the process is shown in Table 2.2 and the mechanism of the reaction is shown in Figure 2.4 (Centi et al., 1988).

Table 2.2: Proposed Steps in the Oxidation of *n*-butane to Maleic Anhydride

Reaction	Type of Reaction
n-butane → 1-butene	Oxidative dehydrogenation
1-butene → 1,3-butadiene	Allylic oxidation
1,3-butadiene → 2,5-dihydrofuran	1-4 Oxygen insertion
2,5-dihydrofuran → Furan	Allylic oxidation
Furan → Butyrolactone	Electrophilic oxygen insertion
Butyrolactone → Maleic Anhydride	Electrophilic oxygen insertion

Butenes, butadiene and furan have been detected in the oxidation of *n*-butane with VPOs catalyst under very unusual conditions, such as in deficiency of oxygen at very high *n*-butane concentration and at very low contact time, under high vacuum in Temporal Analysis of Products (TAP) reactor or in the oxidation of *n*-butane under anaerobic conditions in a pulse reactor (Centi et al., 1988).

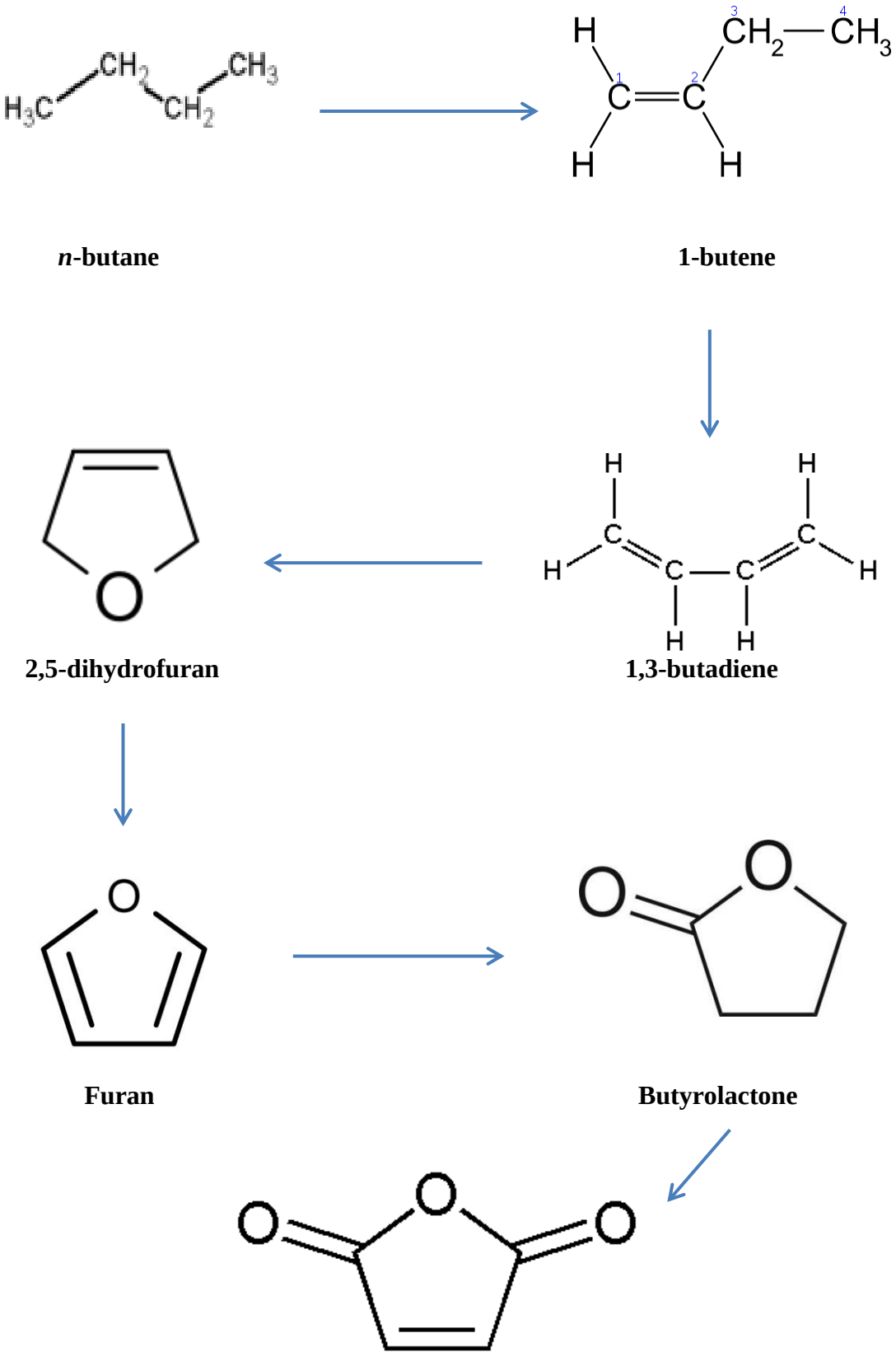

Figure 2.4: Mechanism of *n*-Butane Oxidation

2.6 Worldwide Demand of Maleic Anhydride

In the early 1930s, maleic anhydride (MA) was first commercially produced by the vapour phase oxidation of benzene. In 1974, Monsanto firstly produced MA from butane. However, the use of benzene as the feedstock was dominant in the world market. In the meantime MA was also produced as a by-product in a small amount from the synthesis of phthalic anhydride. In 1978, an estimated value of 341 million pounds of MA was produced (Felthouse et al., 2001).

The global production of MA had grown ever since to an estimated value of 1.8 billion pounds worth USD 700 million in 1995. In the past few years, an average rate of 5.8 % increase throughout the world production of MA. Through the rapid advancement in the catalyst technology, the United States had maximized the usage of butane as feedstock in the production of MA (Felthouse et al., 2001).

Based on the recent report by World Petrochemical (WP), global production and consumption of MA in 2010 were both approximately 1.7 million metric tons. Global capacity utilization was 65 % in 2010, a slight increase from 2009. MA consumption is estimated to increase by 5.7 % in 2012. It is expected to grow an average 5.6 % per year from 2010 to 2015, and 3.5 % per year from 2015 to 2020. Unsaturated polyester resins accounted for an estimated 39 % of global MA consumption in 2010, followed by 1,4-butanediol. Other applications of MA include agricultural chemicals, lube oil additives, fumaric acids and others. These information are summarized in Figure 2.5 (World Petrochemical, 2011).

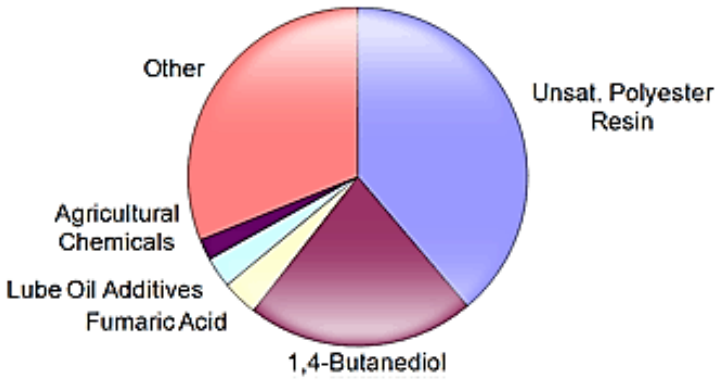

Figure 2.5: World Consumption of Maleic Anhydride - 2010

2.7 Vanadyl Pyrophosphate Catalyst $(VO)_2P_2O_7$

Vanadium pyrophosphate $(VO)_2P_2O_7$ is commercially used as catalyst for the selective oxidation of *n*-butane to maleic anhydride. Vanadium phosphorous oxides (VPO) have also shown promising results as heterogeneous catalysts in the selective oxidation of propane to acrylic acid, pentane to maleic and phthalic anhydride, and in the oxidative dehydrogenation of ethane and propane (Datta et al., 2002).

Vanadium phosphates constitute a very interesting class of layered compounds which exist in a wide range of structural forms both due to the variable valence of vanadium as well as the large diversity in the bonding of the VO_6 octahedron and the PO_4 structural units. Several phases containing vanadium in +5, +4 and +3 oxidation states are known. In all these compounds the layers are held together by hydrogen bonding or by weak Van der Waal's interactions. These layered compounds are therefore amenable for intercalation reactions (Datta et al., 2002).

In the present work we describe different approaches that have been adopted to synthesise novel phases in the VPO system as well as modify the structures of some known catalytically important vanadium phosphate phases. In addition, the catalytic activities of some of these new and modified phases have been investigated (Datta et al., 2002).

The VPO catalysts are prepared by thermal dehydration of its precursor, vanadyl (1V) hydrogen phosphate hemihydrate, $VOHP0_4 \cdot 0.5H_2O$. The catalytic performance of the VPO catalysts depends on:-

1. The method of $VOHP0_4 \cdot O.5H_20$ synthesis (types and concentrations of reagents, reducing agents and solvents, the reduction temperature and synthesis duration).
2. The procedures for activation and conditioning of the precursor at high temperature.
3. The nature of metal promoters.

(Guliants & Carreon, 2005)

2.8 Surface Model of $(VO)_2P_2O_7$

Volta et al., believed that the active sites are not associated with the interfaces between the crystalline phases. The active phase for the selective oxidation of *n*-butane consists of a mixture of well crystalline $(VO)_2P_2O_7$ and an amorphous $VOPO_4$ phase involving corner sharing VO_6 octahedron (Figure 2.6A). This amorphous phase was interpreted as a precursor of β-$VOPO_4$, which formed at higher temperatures. He also suggested that domains of γ-$VOPO_4$ supported on $(VO)_2P_2O_7$ matrix are necessary for selective *n*-butane oxidation (Guliants & Carreon, 2005).

Yamazoe et al., have reported $VO(H_2P0_4)_2$ as the precursor of the active and selective phase in *n*-butane oxidation. This precursor transformed to an amorphous $VO(P0_3)_2$ catalyst which was much less active but just as selective as the $(V0)_2P_20_7$ catalysts. This is shown in Figure 2.6B (Guliants & Carreon, 2005).

Trifiro et al., attributed the activity of the VPO catalysts in *n*-butane oxidation to vanadyl pyrophosphate, whereas the selectivity to maleic anhydride was associated with the presence of a very limited and controlled amount of V^v sites (Figure 2.6C). He also suggested that the active surface is obtained by truncation of the $(VO)_2P_20_7$ crystals along the (1 0 0) plane (Guliants & Carreon, 2005).

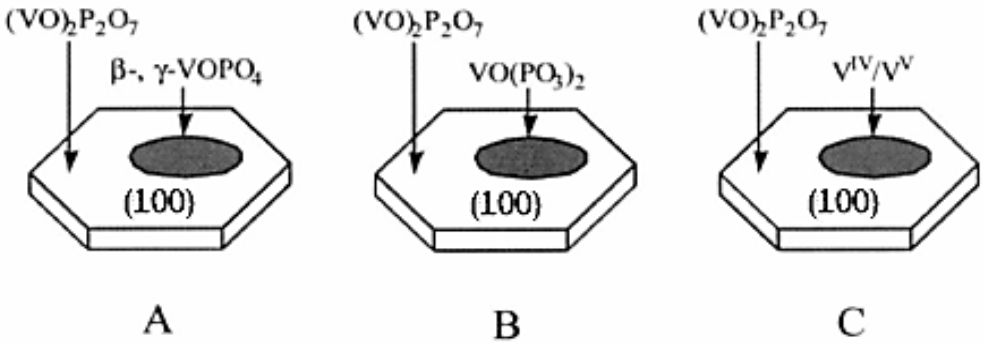

Figure 2.6: Models of the active surface of the VPO catalyst according to:-

A : Volta et al., (1991)	B : Yamazoe et al., (1990)	C : Trifiro et al., (1988)

On the basis of these observations, there is a general agreement that the best model of the surface catalyst is obtained by truncation of the catalyst of the crystals along the planes parallel to the (1 0 0) plane (Figure 2.7). On the other hand, truncations of the side (0 2 1) and (0 0 1) planes were first taken by Matsuura and Yamazaki (1990) and later by Volta et al., (1992) and Okuhara et al., (1993) as a model for the site active in the non-selective of *n*-butane (Cavani & Trifiro, 1990).

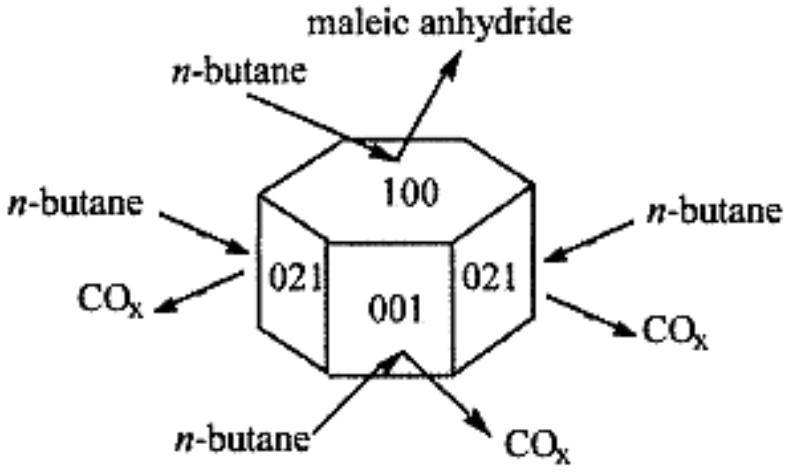

Figure 2.7: Selective and Non-selective Oxidation Sites on the Crystal Faces of $(VO)_2P_2O_7$

2.9 Preparation of the Vanadium Phosphorus Oxide Catalyst (VPO)

Generally there is two routes to prepare the VPO catalyst, namely Hemihydrate Route and Sesquihydrate Route. Hemihydrate route is further divided into Organic medium, Aqueous medium and Dihydrate route.

2.9.1 Hemihydrate Route

Vanadyl (IV) hydrogen phosphate hemihydrate, $VOHPO_4 \cdot 0.5H_2O$ is the common precursor of the VPO catalysts for the selective oxidation of *n*-butane to maleic anhydride. The hemihydrate is usually prepared by refluxing its component oxides in alcohol.

Vanadyl pyrophosphate $(VO)_2P_2O_7$, the active phase of VPO catalysts is usually obtained by the thermal treatment of the hemihydrate precursor in a mixture of *n*-butane in air (Guliants & Carreon, 2005).

Organic Route:

15 g of V_2O_5 (Sigma) was suspended by rapid stirring into 90 mL of isobutyl alcohol and 60 mL of benzyl alcohol. The vanadium oxide-alcohol mixture was refluxed for 3 hours at 120°C under continuous stirring. During this period the solution changed colour from brown to black.

The mixture was then cooled to room temperature and left stirring at this temperature overnight. 99 % *o*-H_3PO_4 was added in a quantity such as to obtain the expected P/V atomic ratio. The resulting solution was again heated to 120°C and maintained under reflux with constant stirring for 2 hours.

Then the slurry (precursor) was filtered, washed, and dried at 150°C. This precursor was calcined in air at 400°C for 6 hour and then for an additional 3 hour in a mixture of 0.75 % *n*-butane and air (Taufiq Yap et al., 2001).

Aqueous Route:

15 g of V_2O_5 (Sigma) was dissolved in 200 mL of 37 % HCl. The solution was refluxed and stirred until complete reduction to vanadium (IV) (about 3 hours). Then 85 % *o*-H_3PO_4 was added to obtain the desired P/V atomic ratio; at this stage, no precipitation occurs because the solution is strongly acidic.

This solution was allowed to boil for 2 hours and concentrated to a volume of 20 mL to which hot water was then added to obtain blue vanadyl orthophosphate. After evaporation, the solid (precursor) was dried at 150°C overnight, and then calcined as described in the previous method (Taufiq Yap et al., 2001).

Dihydrate Route:

V_20_5 reacting with H_3PO_4 (30 ml, 85 %) in water under reflux for 24 hours. Yellowish solid, $VOPO_4 \cdot 2H_2O$ is recovered by filtration and washed with water followed by acetone. The $VOPO_4 \cdot 2H_2O$ reacted with isobutanol and reflux for 20 hours.

The solid product was recovered by filtration and dried in air. This vanadyl phosphate hemihydrate precursor then later activated to vanadium phosphorus oxide (VPO) (Taufiq Yap et al., 2004).

2.9.2 Sesquihydrate Route

Recently, an alternative route in producing vanadyl pyrophosphate catalyst has been developed via vanadyl hydrogen phosphate sesquihydrate precursor ($VOHPO_4 \cdot 1.5H_2O$). The synthesis of sesquihydrate precursor has been divided into a two-step procedure involving $VOPO_4 \cdot 2H_2O$ as an intermediate before obtaining the precursor.

In the first step:

Vanadyl phosphate dihydrate, $VOPO_4 \cdot 2H_2O$ was prepared by reacting V_2O_5 (12.0 g from Fischer) with aqueous *o*-H_3PO_4 (115.5 g, 85 % from Fischer) in distilled water (24 ml g−1 solid). The mixture was then stirred under reflux at 393K for 24 h. The brownish solid solution (colour of V_2O_5) has gradually changed to yellow.

The resultant yellow solid ($VOPO_4 \cdot 2H_2O$ phase) was then recovered by using centrifuge technique and subsequently washed sparingly with distilled water and oven dried at 353K for 16 h.

In the second step:

10.0 g of $VOPO_4 \cdot 2H_2O$ (50.5 mmol) was added to 150 ml of 1-butanol (PC Laboratory Reagent) and refluxed at 353K for 24 h. After cooled to room temperature, the resultant precipitates which is whitish-blue powder ($VOHPO_4 \cdot 1.5H_2O$) was centrifuged out from the solvent, washed sparingly with acetone, and dried overnight (24 h) in an oven at 353 K. The sesquihydrate precursor obtained was calcined at 673K in a reaction flow of 0.75 % *n*-butane/air mixture (Taufiq Yap et al., 2004).

2.10 Parameters of the Vanadium Phosphorus Oxide Catalyst (VPO)

There are six parameters which attribute to the activity and selectivity of VPO catalyst in the selective oxidation of *n*-butane to maleic anhydride. These parameters are:-

1. Doped system
2. Support system
3. Calcination temperature
4. Calcination duration
5. Calcination environment
6. P/V atomic ratio

By altering these parameters, the performance of the VPOs catalyst can be increased or decreased depending on the interactions of these parameters with the VPOs catalyst performance and how these parameters are altered.

2.10.1 Doped System

Dopant is the additives which have an effect of the operation of the catalysts. Some additives have the opposite effect, which are known as catalyst poison. Dopant or known as promoters is the chemicals added into the catalyst during preparation in a small amount to enhance the activity, selectivity or stability of the catalyst.

Dopant by itself is low in activity and inactive. With the addition of the proper dopant, an increase in the activity is achievable and this reduces the cost of production and the operation becomes more economic (Cheng, 1996 and Felthouse et al., 2001).

Normally, the promoters added have basic nature that they can easily donate electrons to the framework of vanadyl phosphate. The incorporation of such alkali or alkaline-earth metal ions would donate electrons to the V-P-O lattice with P/V ratios of 1.07 and 1.20 giving the rise of negative charge on the lattice oxygen atoms. This was determined by Zazhigalov et al., (1996) and was found that the conversion of *n*-butane is enhanced.

Basically there are three functions of promoter:-

1. Textural promoters inhibit the growth of the small particles of the active phase during usage
2. Electronic or structural promoter may dissolve in the active phase and alters its electronic character
3. Poison resistant promoters protect the active phase against poisoning by impurities in the reactants or generated by side reactions

(Bond, 1987)

Particularly in the selective oxidation of *n*-butane to maleic anhydride over the VPOs catalyst, the promoters have twofold structural role namely; to enable the formation of the required VPOs compounds and decrease the formation of deleterious phases. Besides, it also enables the formation of solid solutions that regulate the catalytic activity of the solid (Taufiq Yap et al., 2006).

2.10.2 Support System

Catalyst supports are normally porous metal oxides which have high surface area or carbons that have significant pore volume and capacity for preparing and preserving stable, well-dispersed catalytic phases during catalytic reaction. Hence, supports are used to provide a very large surface area for the catalyst (Bartholomew & Farrauto, 2005).

Among all, alumina, silica and carbon are the most common with magnesia, zirconia, zeolites and silicon carbide used in certain applications. They are commonly used in the industrial catalytic processes because of their wide range of chemical and physical properties as well as excellent thermal stability (Bartholomew & Farrauto, 2005).

Supported VPO catalysts are more favourable compared with the unsupported ones since they have better heat transfer character, larger surface area to volume ratio of active component, controllable catalyst textures and better mechanical strength. It is noticed that, the existence of a support can result in support-oxide interaction that may hinder the formation of $(VO)_2P_2O_7$ phase or bring about changes in phase composition (Ruiteenbeek et al., 1998).

It has been reported that V^{5+} containing phase, such as α-$VOPO_4$ or γ-$VOPO_4$, exists in supported VPO catalysts, especially in those prepared in aqueous media, and that the presence of such phases may lower *n*-butane conversion and/ or MA selectivity (Ruiteenbeek et al., 1998).

2.10.3 Calcination Temperature

Calcination is a high-temperature treatment of catalyst precursors in air which is usually the final step in producing oxide catalysts or the second-last step in producing metal catalysts. The main purpose of carrying out calcination is to decompose and volatilize various volatile impurities or catalyst precursors formed during the preparation process. They are normally not the desired forms for the final catalysts like hydroxides, nitrates and carbonates (Bartholomew & Farrauto, 2005).

A fresh catalyst has been designated as a non-equilibrated one, while a catalyst after a prolonged time on stream has been designated as an equilibrated one. A non-equilibrated catalyst is more active and has lower selectivity to maleic anhydride, especially at high conversion, owing to the easier oxidation of V^{4+} to V^{5+}.

According to Ebner and Thompson, an equilibrated catalyst is the one that has been in a flow on a stream with a hydrocarbon for approximately 200 to 1000 hours. One of the main properties of an equilibrated catalyst is the presence of stable V^{4+}. Equilibrated catalysts are no longer re-oxidizable in air at 400ºC, contrary with a non-equilibrated catalyst.

The catalytic selectivity towards the desired product is dependent on the availability of acid sites. Nevertheless, the adsorption diminishes by effect of calcinations temperature due to the loss of functional groups of vanadyl pyrophosphate phase (Ebner & Thompson, 1993).

2.10.4 Calcination Duration

Calcination duration refers to the time the precursor is activated in the reactor. Most of the precursors are activated over duration of 6 hours. Increasing the time of calcination will lead to an increase in the surface area of the catalyst, since the precursors are in contact with the flowing gas for a longer duration (Taufiq Yap et al., 2001).

However, the longer the duration of the calcination, the higher probability of the rosette structure to be agglomerated. Moreover, the $VOPO_4$ phase in the catalyst is also completely removed. This also occurs in the short calcination duration, but only in a small amount (Taufiq Yap et al., 2001).

2.10.5 Calcination Environment

Calcination environment refers to the calcination gas used to activate the catalyst. When calcined in different environment, the resulting catalysts after activation will show different activity and selectivity. The vanadium valence of the catalyst increases with increasing oxidizing potential of the calcination gas. The selectivity to maleic anhydride and specific activity increases with the vanadium valence, but the surface area decreases with the vanadium valence (Cheng, 1996).

Amorphous V^{5+} species in the working catalyst will be readily hydrated. The phase evolution during the thermal dehydration of the hydrate is similar to that of α-$VOPO_4 \cdot 2H_2O$. The oxidation reaction will not result in surface enrichment of V^{5+} relative to V^{4+}. The calcination atmosphere affects the catalyst morphology and the vanadium valence. An unpromoted VPO catalyst is more resistant to oxidation than the promoted catalyst in calcination, and achieves its optimized maleic anhydride yield when calcined in a more oxidizing atmosphere (Cheng, 1996).

The study suggests that dispersed V^{5+} species in contact with $(VO)_2P2O_7$ is important for the oxidation of *n*-butane to maleic anhydride. Calcination atmospheres need to be chosen in accordance with the oxidizability of the VPO catalyst precursors to achieve the optimized performance (Cheng, 1996).

2.10.6 P/V Atomic ratio

Optimal catalyst composition presents a slight excess of phosphorus with respect to the stoichiometric value of the precursor. There is a general agreement that a high P/V atomic ratio helps in avoiding the oxidation of V^{4+} in $(VO)_2P_2O_7$.

In catalyst with a slight defect of phosphorus (P/V =0.95), a considerable increase of the ease of oxidation occurs and the reducibility remains high. For P/V atomic ratio higher than 1, both the re-oxidizability and the reducibility decrease considerably. It is found that high relative amounts of V^{5+} increase the activity and decrease the selectivity. While low reducibility of V^{4+} is an index of low activity.

Catalyst with slight excess of phosphorus (P/V=1.05) exhibit the right compromise between reducibility and re-oxidizability necessary to obtain both high activity and high selectivity. According to Matsuura and Yamazaki, the excess phosphorus avoids the oxidation of the catalyst by forming on the side faces of the (1 0 0) plane a $(VO)(PO_3)_2$ phase, characterized by a lower oxidizability.

CHAPTER 3

METHODOLOGY AND CHARACTERIZATION TECHNIQUES

3.1 Materials

Chemicals that were used in this project are as follows:-

1. Vanadium (V) pentoxide, V_2O_5 (Merck)
2. *ortho*-Phosphoric acid, *o*-H_3PO_4 (R&M Chemicals)
3. 1-butanol, $CH_3(CH_2)_3OH$ (R&M Chemicals)
4. Sulphuric acid, H_2SO_4 (95-98 %) (Merck)
5. Potassium permanganate, $KMnO_4$ (Fisher Scientific)
6. Ammonium iron (II) sulphate, $(NH_4)Fe(SO_4)_2$ (R&M Chemicals)
7. Diphenylamine, Ph_2NH (ACROS)
8. Nitric acid, HNO_3 (R&M Chemicals)

The gases used in this project are as follows:-

1. 0.75 % *n*-butane in air (Malaysia Oxygen Berhad, MOX)
2. 99.99 % Purified Nitrogen (Malaysia Oxygen Berhad, MOX)
3. 99.99 % Purified Helium (Malaysia Oxygen Berhad, MOX)
4. Liquefied Nitrogen Gas (Malaysia Oxygen Berhad, MOX)

3.2 Methodology

In this research, the bulk catalyst is prepared via sesquihydrate route. There are total of four stages involved in prepared the catalyst, namely Stage 1, Stage 2, Stage 3 and finally Stage 4. A brief explanation on how each stage is carried out along with a diagram flow is shown to provide a better understanding of the on-going process.

3.2.1 Preparation of the Dihydrate precursor

In Stage 1, 2.5 g of Vanadium pentoxide, V_2O_5 (Merck), is added with 60 ml of distilled water and 15 ml of *ortho*-Phosphoric acid, *o*-H_3PO_4. The solution is stirred using a spatula and placed in microwave digester at a temperature of 140ºC for 2 hours. The yellowish precipitate obtained is centrifuged to separate the slurry mixture. The slurry is then evenly spread on ceramic bowls and covered with aluminium foil. It is then placed in the oven to be dried at approximately 90ºC for 24 hours (Figure 3.1).

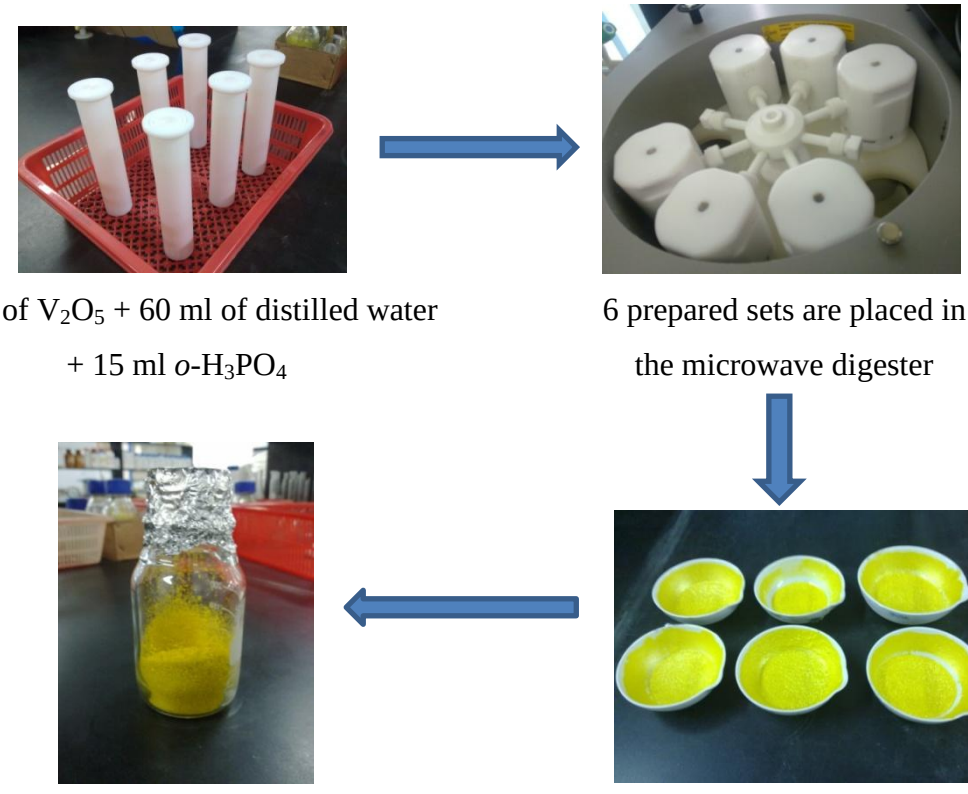

Figure 3.1: Flow Diagram of Dihydrate Preparation Route

3.2.2 Preparation of the Sesquihydrate precursor

As for Stage 2, 10 g of $VOPO_4 \cdot 2H_2O$ (obtained from Stage 1) is added with 233 ml of 1-butanol (R&M Chemicals) and stirred using a spatula. The mixture is then undergone reflux for 6 hours, followed by cooling to room temperature overnight. After which it is centrifuged and oven dried at 90ºC for 24 hours. The resultant whitish-blue precipitate powder obtained is the sesquihydrate precursor (Figure 3.2).

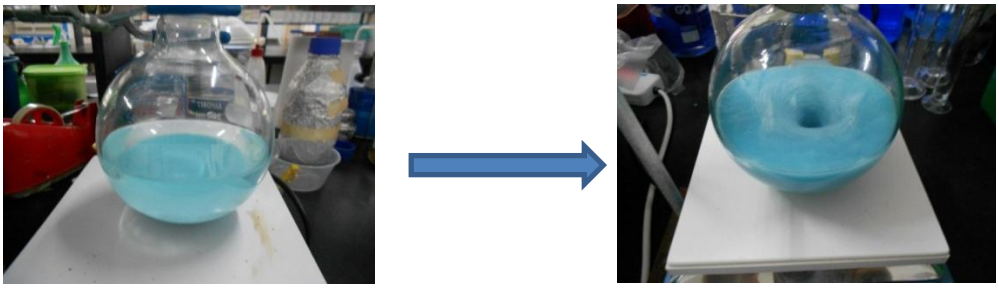

10 g of $VOPO_4 \cdot 2H_2O$ + 233 ml 1-butanol

Refluxed at 400 K for 6 hours

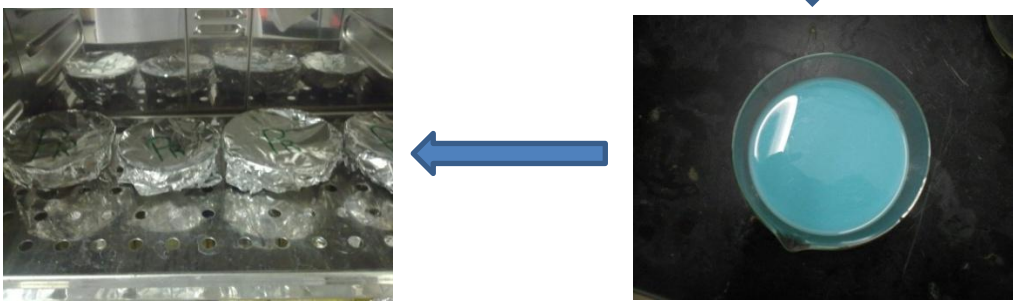

Mixture collected after cooling to room temperature

After centrifuged, the samples are placed in the oven overnight

Figure 3.2: Flow Diagram of Sesquihydrate Preparation Route

3.2.3 Doping

In Stage 3, the calculated amount of dopant is prepared in a glass bowl. 10 ml of 1-butanol (R&M Chemicals) is added and the mixture is physically stirred on the hot plate while the heat function on the stirrer is turned on.

Once a homogenized mixture is observed, the heater power is turned off and the $VOHPO_4 \cdot 1.5H_2O$ (obtained from Stage 2) is added and stirred physically. When a homogenized solution is observed, the mixing is stopped and the glass bowl is aluminium foiled. It is then placed in the oven to be dried overnight (Figure 3.3).

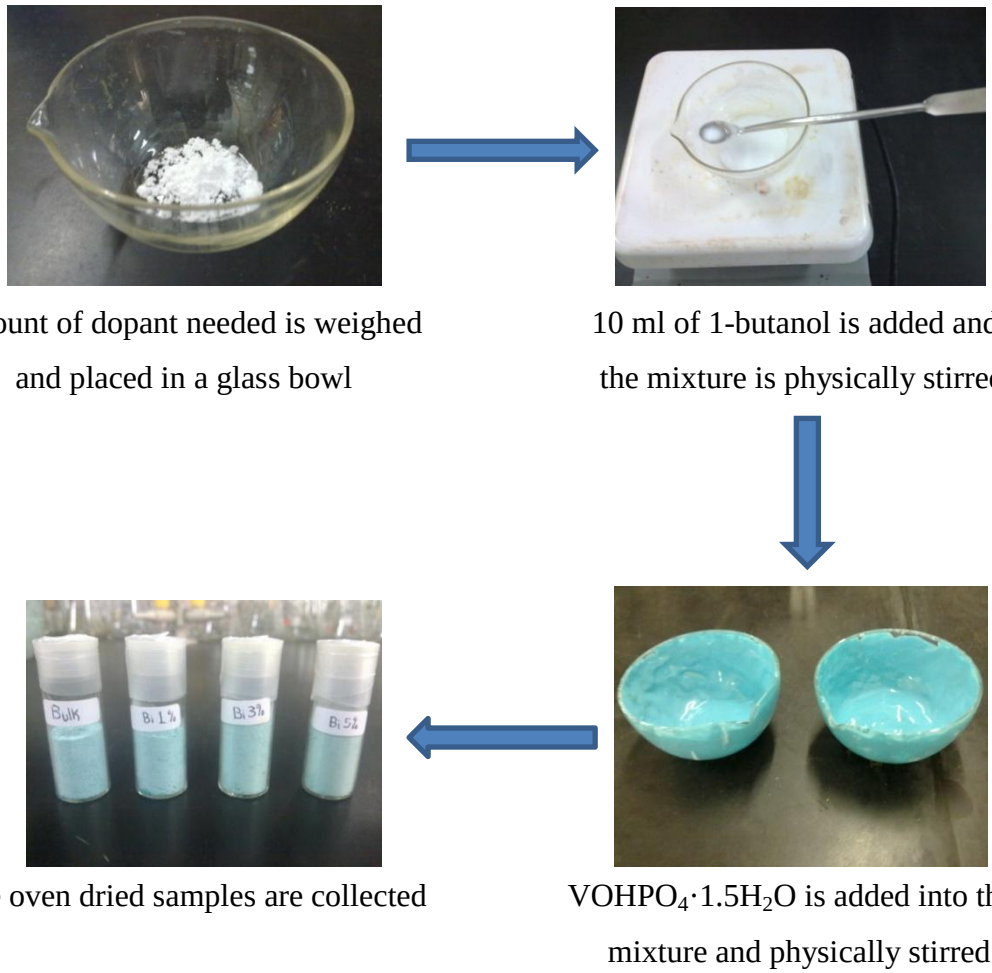

Figure 3.3: Flow Diagram of Doping the Sesquihydrate

3.2.4 Calcination

The doped precursor is placed on 6 boats. A straight line is drawn between the powders in each boat to enhance the contact area of the gas. These boats are placed on a holder which is then placed into the calcination reactor. The doped precursor is calcined for 6 hours at 460ºC. After letting it cool down to below 50 ºC, the sample is collected. These steps are repeated for all four doped precursors (Figure 3.4).

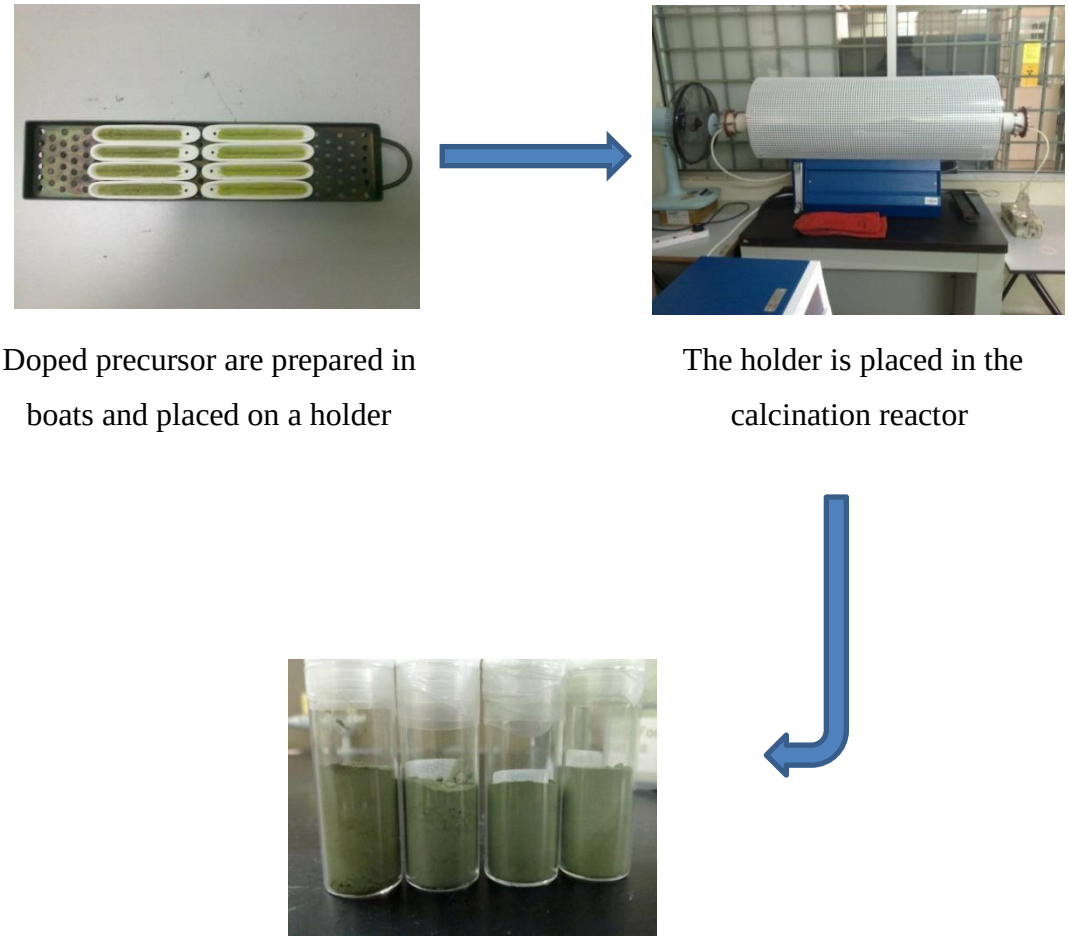

Doped precursor are prepared in boats and placed on a holder

The holder is placed in the calcination reactor

Sample collected and stored after calcination

Figure 3.4: Flow Diagram for the Calcination of the Doped Precursor

3.3 Characterization Techniques

After the synthesis stage, the prepared catalyst needs to under several test to determine its physical and chemical properties. These test are carried out using the following equipment's:- X-Ray Diffractometer (XRD), BET Surface Area Measurement, Scanning Electron Microscopy with Energy Dispersive X-ray (SEM-EDX), Redox Titration and Temperature Program Reduction (TPR).

3.3.1 X-Ray Diffractometer (XRD)

The model of XRD analysis machine used in this research is Shimadzu XRD-6000 Diffractometer (Figure 3.5). The XRD-6000, an X-ray diffractometer analyse crystalline states under normal atmospheric conditions. This method is non-destructive.

X-rays focused on a sample fixed on the axis of the spectrometer (goniometer) are diffracted by the sample (Figure 3.6). The changes in the diffracted X-ray intensities are measured, recorded and plotted against the rotation angles of the sample. The result is referred to as the X-ray diffraction pattern of the sample (Shimadzu Corporation, 2007).

Figure 3.5: Shimadzu XRD-6000 Diffractometer

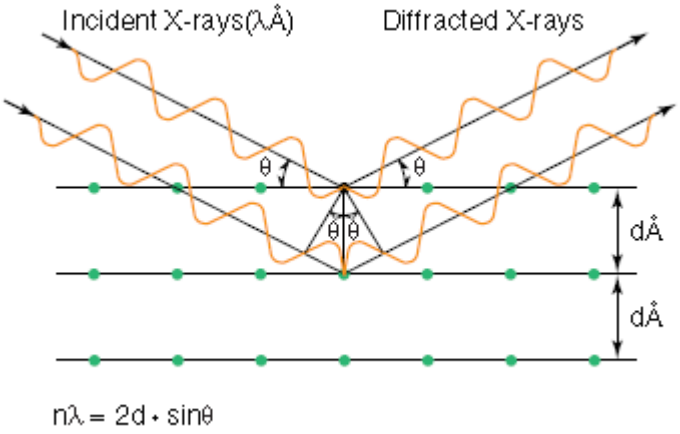

Figure 3.6: Incident x-rays and diffracted x-rays

Computer analysis of the peak positions and intensities associated with this pattern enables qualitative analysis, lattice constant determination and/or stress determination of the sample. Qualitative analysis may be conducted on the basis of peak height or peak area. The peak angles and profiles may be used to determine particle diameters and degree of crystallization, and are useful in conducting precise X-ray structural analysis (Shimadzu Corporation, 2007).

The crystallite size determined by the XRD method can be explained by the Debye Scherer equation:-

$$t = \frac{0.89\lambda}{\beta_{hkl} \cos \theta_{hkl}} \qquad (3.1)$$

Where:-

t = crystallite size for (h k l) plane

λ = X-ray wavelength of radiation for CuKα

β_{hkl} = full width at half maximum (FWHM) (h k l) plane

θ_{hkl} = diffraction angle for (h k l) plane

3.3.2 BET Surface Area

Brunauer-Emmett-Teller (BET) surface area is used for the determination of the multi-point surface area of porous materials using the analysis machine, Thermo Finnigan Sorptomatic 1990 (Figure 3.7). Clean solid surface adsorbs surrounding gas molecules BET theory provides a mathematical model for the process of gas sorption. This physical adsorption of gas over the entire exposed surface of a material and the filling of pores is called physisorption and is used to measure total surface area and pore size analysis (Yuan et al., 2010).

Figure 3.7: Thermo Finnigan Sorptomatic 1990

BET surface area measurement is crucial in understanding the behaviour of a material, as material reacts with its surrounding via its surface, a higher surface area material is likely to react faster, dissolve faster and adsorb more gas than a similar material with lower surface area (Yuan et al., 2010).

The concept of the theory is an extension of the Langmuir theory, which is a theory of monolayer adsorption to multilayer adsorption with the following hypothesis:-

1. Gas molecules physically absorb on a solid in layers infinitely
2. There is no interaction between each adsorption layer
3. Langmuir theory can be applied to each layer

The resulting BET equation is expressed by:-

$$\frac{1}{v[\left(\frac{P_0}{P}\right)-1]} = \frac{c-1}{v_M c}\left(\frac{P_0}{P}\right) + \frac{1}{v_M c} \qquad (3.2)$$

Where:-

P = equilibrium pressure of adsorbate at the temperature of adsorption

P_0 = saturation pressure of adsorbate at the temperature of adsorption

v = adsorbed gas quantity

v_M = monolayer gas adsorbed quantity

c = BET constant

$= \exp\left(\frac{E_1 - E_L}{RT}\right)$; where:-

E_1 = the heat of adsorption in the first layer

E_L = heat of adsorption of the second and higher layer and is equal to the heat of liquefaction

3.3.3 Scanning Electron Microscopy (SEM)

In this research, the Hitachi S-3400N (Figure 3.8) is used as the analysis machine to determine the catalyst structure as well as the elemental composition. It incorporates both the scanning electron microscope and the energy dispersive x-ray.

Figure 3.8: Hitachi S-3400N

Electron microscopy techniques have been used to obtain information on the morphology and size of the VPO crystallites by scanning electron microscopy (SEM). In the SEM, an electron beam is focused into the fine probe and subsequently raster scanned over a small rectangular area. As the beam interacts with the sample, various signals are created and these signals are high localised in the area directly under the beam.

Using these signals to modulate the brightness of a cathode ray tube, which is raster in synchronization with the electron beam, an image is formed on the screen. This image can be magnified and has a traditional microscopic image look, but with a greater depth of field.

3.3.4 Energy Dispersive X-ray (EDX)

Energy dispersive x-ray analysis is used to view the surface and for chemical analysis of the microstructure component. The EDX machine is coupled together with the SEM machine, so that parameters that affect the x-ray spectrum such as current probe, process time and dead time can be manipulated and analysed.

This is an analytical technique used to determine the elements in a sample or characterize them chemically. The basic fundamental of EDX is that each element has a unique atomic structure which results in unique sets of peaks when stimulated by x-ray spectrum.

X-ray beam is focused on the sample being studied, which excites and emits an electron from the inner shell creating an electron hole. The electron from the outer surface fills the hole and the difference in energy between the higher energy shell and lower energy shell is emitted as x-ray. The number and energy of the x-rays emitted is measured using by an energy dispersive spectrometer.

The elemental composition of the sample is determined from the energy of the x-ray, as it contains information on the difference in the energy between the two shells, and the atomic structure of the element from which they were emitted from.

3.3.5 Redox Titration

In 1982, Miki Niwa and Yuichi Murakami developed the redox titration method. 10 g of the catalyst sample is dissolved in sulphuric acid (2M). The V^{III} and V^{IV} in solution oxidize to V^{V} with the addition of potassium permanganate solution. The end point is indicated by the change of colour from greenish-blue to pink. Volume of the potassium permanganate used was recorded, V_1 (Niwa and Murakami, 1982).

A fresh solution was titrated by ammonium iron (III) sulphate with diphenylamine as an indicator to determine the V^V content. Changes in the solution colour from purple to greenish-blue indicate the end point. Volume of ammonium iron (III) sulphate used was recorded, V_2 (Niwa and Murakami, 1982).

The oxidized solution is then reduced by ammonium iron (II) sulphate with diphenylamine as the indicator. When the colour of the solution changes from purple to colourless, the end point is reached. The amount of ammonium iron (II) sulphate solution used is recorded as V_3 (Niwa and Murakami, 1982).

The respective concentration of the vanadium species in the catalyst can be determined by the following equation:-

$$(2V^{3+} + V^{4+})(V_a) = [MnO_4^-](V_2) \quad (3.3)$$

$$(V^{3+} + V^{4+} + V^{5+})(V_b) = [Fe^{2+}](V_2) \quad (3.4)$$

$$(V^{5+})(V_c) = [Fe^{2+}](V_3) \quad (3.5)$$

(Niwa and Murakami,1982).

Where:-

V^{3+}, V^{4+} V^{5+}	= concentration of the vanadium species in different oxidation state
$[MnO_4^-]$	= concentration of the potassium permanganate solution
$[Fe^{2+}]$	= concentration of the ammonium iron (II) sulphate solution
V_1	= volume of the potassium permanganate used
V_2, V_3	= Volume of the ammonium iron (II) sulphate solution used
V_a, V_b, V_c	= Volume of the catalyst solution used

The average oxidation state of vanadium (AV) obtained by solving the equation below:-

$$V_{AV} = \frac{3V^{3+} + 4V^{4+} + 5V^{5+}}{V^{3+} + V^{4+} + V^{5+}} \quad (3.6)$$

(Niwa and Murakami,1982).

3.3.6 Temperature Program Reduction (TPR)

Temperature programmed method was developed in which a catalyst is subjected to a linear temperature raise in a flow of diluted hydrogen. Hydrogen is being consumed as the catalyst is being reduced. A thermal conductivity detector is used to measure the change in the thermal conductivity of the gas mixture before and after the reaction. Due to the initiation of reduction at various thermal energy levels, several reduction peaks will be detected over the course of the temperature ramp (Figure 3.9).

Figure 3.9: TPD/R/O 1100

In the TPR analysis a mixture of reactive gas with inert gas, 5.55 % hydrogen in nitrogen is flown through a sample which is pre-treated. The hydrogen gas will reduce the sample and the hydrogen consumption will be can be monitored through the TCD detector. The objectives of the TPR technique are the following:

1. To characterize complex systems, such as bimetallic and doped catalyst
2. To determine the role of second component
3. Establish alloy formation or promotion effects
4. To find the most efficient reduction conditions
5. Identify the supported precursor phases and their interactions with the support
6. To investigate different types of oxygen species present in the catalyst, which may be involved in the oxidation process

In the TPR analysis, 0.3 g of catalyst is weighed into the reactor and connected to the preparation port. Pre-treatment process is carried out by flowing the 5.55 % of hydrogen in nitrogen (H_2/N_2) gas to remove the moisture from the sample. The catalyst is cleaned by heating it at 10 K min^{-1} from room temperature to 473 K in a purified nitrogen flow at 25 cm^3 min^{-1}.

The flow is maintained at 473 K for 30 minutes before cooling to ambient temperature. After which the flow is switched to 5.23 % H_2/Ar at 25 cm^3 min^{-1}. The thermal conductivity difference between the reactant and the carrier gas is optimized by the composition of the reducing gas. Temperature is raised at 10 K min^{-1} to 1273 K following the conductivity of the eluted gas. TPR profile is a plot of hydrogen consumption of a catalyst as a function of time, which is converted to a function of temperature.

CHAPTER 4

RESULTS AND DISCUSSION

4.1 Introduction

The physical and chemical properties of Vanadyl Pyrophosphate Catalyst (VPOs) calcined with different percentage of bimetallic dopants have been scrutinized under various instrumental analyses, namely:-

1. X-Ray Diffraction (XRD) Analysis
2. Brunauer-Emmett-Teller (BET)
3. Scanning Electron Microscopy (SEM)
4. Energy Dispersive X-Ray Diffraction (EDX)
5. Redox Titration
6. Temperature Program Reduction (TPR)

The catalysts obtained via calcination of different percentage of dopants are denoted as: VPOs-Ba5, VPOs-Ba5,Bi1, VPOs-Ba5,Bi3 and VPOs-Ba5,Bi5.

4.2 X-Ray Diffraction (XRD) Analysis

The XRD patterns of the four catalysts obtained via calcination of different percentage of bimetallic dopants at 733 K under the flow of 0.75 % *n*-butane in air is shown in Figure 4.1. The catalysts are characterized according to the peaks appearing at 2θ = 22.9°, 28.4° and 29.9°, where each of the aforementioned corresponds to (0 2 0), (2 0 4) and (2 2 1) plane respectively.

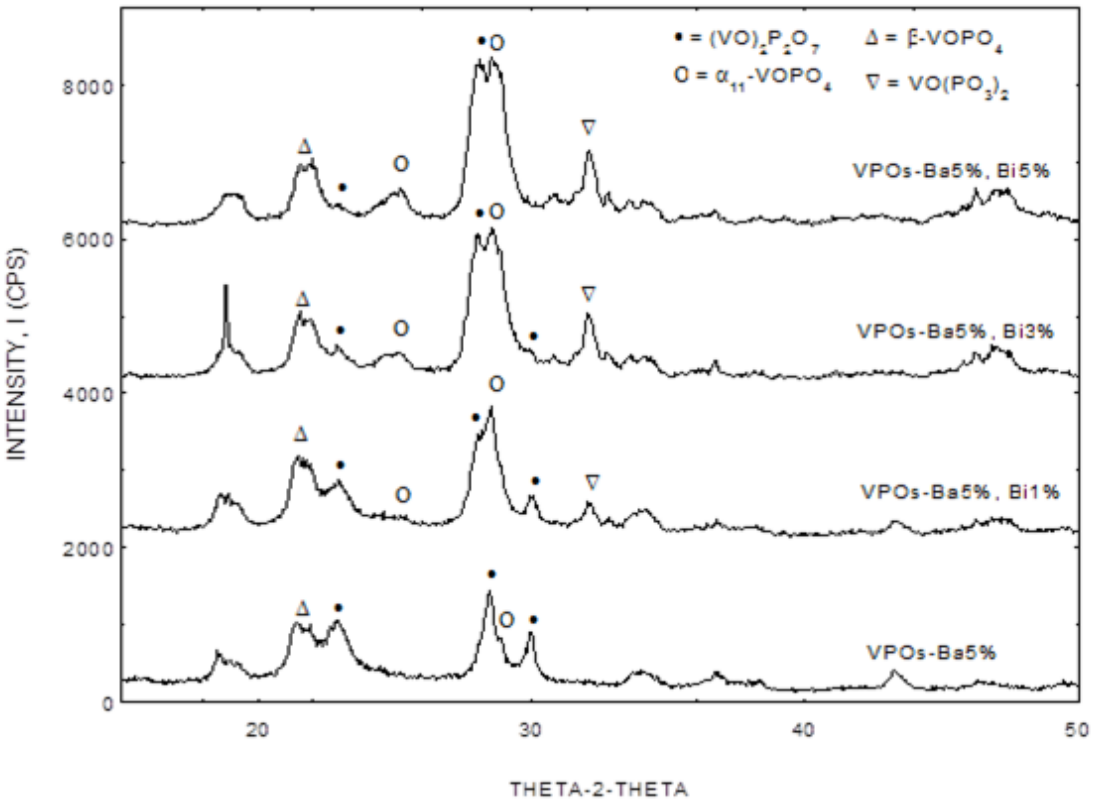

Figure 4.1: XRD Profiles for Different Percentage of Bimetallic Dopants

From the figure above, it is seen that the peaks obtained are not well segregated and there are overlapping peaks. As can be seen in the in the figure, all the catalysts showed similar diffraction pattern comprised of a well crystallized $(VO)_2P_2O_7$ phase with the main characteristics peaks appeared at 2θ = 22.9°, 28.4° and 29.9° (JCPDS File No. 34-1381), which is referring to the reflection of (0 2 0), (2 0 4) and (2 2 1) planes respectively.

As the addition of bismuth increased, the peak at 22.9° is seen to decrease in intensity, while the peak at 28.4 is over shadowed by another peak. The peak at 29.9° is seen deteriorating till it is not seen in the XRD profile for the VPOs-Ba5,Bi5. The conclusion that can be deduced from this is that the addition of bismuth lowers the formation of V^{4+} phase.

Some insignificant peaks were found in the sample appearing at 2θ = 21.5° which corresponds to β-$VOPO_4$ phase (JCPDS File No. 27-0948), at 2θ = 25.1° and 28.7° which represents α_{11}-$VOPO_4$ phase (JCPDS File No. 34-1247) and at 2θ = 32.0° which corresponds to $VO(PO_3)_2$ phase (JCPDS File No. 34-1433). As the percentage of bismuth addition is increased, the peaks belonging to the various V^{5+} phases mentioned above is more intense. This indicates that addition of bismuth to the catalyst promotes the formation of V^{5+} phase component in the catalyst. This is supported by the similar findings by Leong et al., (2011) in "The effect of Bi promoter on vanadium phosphate catalyst synthesized via sesquihydrate route".

Different types of V^{5+} phases have been identified in this research. Key factors in the catalyst preparation to avoid the oxidation of $(VO)_2P_2O_7$ and the intermediate amorphous phase to various $VOPO_4$ phases are as follows:

- P/V ratio in the precursor higher than in the stoichiometric stabilizes the $(VO)_2P_2O_7$ not only in the reactant atmosphere but also in the calcination in air at high temperatures.
- Minimizing the impurities. Small traces of V_2O_5 or additives such as Bi^{3+} facilitate the oxidation of pyrophosphates in the reactant atmosphere.
- Morphology. It had been proposed that the oxidation of starts at the side faces of the (1 0 0) plane. Catalysts with higher exposure of this plane are less oxidized.
- Precursors which contains defects transform at low temperatures than those that are more crystalline

(Trifiro, 1998)

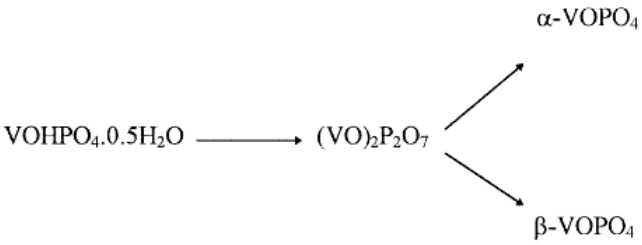

Figure 4.2: Oxidation of pyrophosphate phases in this research

Figure 4.2 shows α-$VOPO_4$ and β-$VOPO_4$ phase which are observed in the XRD analysis. It is also to be noted that, these are not the only two phases that the $(VO)_2P_2O_7$ can oxidize into. Excess of phosphorus on the surface of phosphates is a general phenomenon. Hence, according to Morishige et al., (1990), the excess of phosphorus would be due to the presence of $VO(H_2PO_4)_2$ on the surface of the precursor leading after thermal treatment to $VO(PO_3)_2$ over $(VO)_2P_2O_7$.

The crystallite size of the catalyst is calculated using the Debye-Scherrer equation, given as follow:

$$t(\text{Å}) = \frac{0.89\lambda}{\beta_{hkl}\, x \cos\theta_{hkl}} \qquad (4.1)$$

where t = crystallite size for (h k l) plane in unit Angstrom

λ = X-ray wavelength of radiation for CuKα

β_{hkl} = Full width at half maximum for the (h k l) plane

Θ_{hkl} = Diffraction angle for the (h k l) plane

To determine whether it is vanadyl pyrophosphate phase, the three main peaks are considered, which reflect the (0 2 0), (2 0 4) and (2 2 1) planes. However, the parameter used to determine the crystallite size is the half width of the (0 2 0) and (2 0 4) planes. For the (0 2 0) plane, as the addition of bismuth increases, FWHM (°) decreases and the crystallite size increases. However, the crystallite size for the (2 0 4) plane decreases since addition of bismuth increases the FWHM (°).

It can be deduced that the incorporation of bismuth into the VPOs have shown to produce catalyst with larger crystallite size in the (0 2 0) direction, but smaller in the (2 0 4) direction. Hence, as the line width decrease, crystallite size increases. The calculated result is tabulated in Table 4.1 (Leong et al., 2011).

Table 4.1: XRD Data for VPOs Catalysts with Different Percentage of Doping

Catalyst	FWHM (°)		Crystallite Size (Å)	
	(0 2 0)	(2 0 4)	(0 2 0)	(2 0 4)
VPOs-Ba5	1.1070	0.7401	72.337	109.437
VPOs-Ba5,Bi1	0.9846	1.0788	81.402	75.066
VPOs-Ba5,Bi3	0.9120	1.4363	87.838	56.388
VPOs-Ba5,Bi5	0.6328	1.4719	126.683	55.023

When compared the data obtained with the XRD data for catalyst prepared via the conventional method, the particle thickness at (0 2 0) and (2 0 4) plane catalyst prepared via microwave heating is generally smaller compared to the catalyst prepared via conventional method (Table 4.2). A possible explanation for this is the usage of different reducing agent. In the conventional method, the catalyst is prepared via dihydrate route where isobutanol is used while the catalyst prepared via microwave method implies sesquihydrate route and uses 1-Butanol.

Even though both the planes have smaller crystallite sizes compared to the catalyst prepared via conventional method, only (0 2 0) plane is most important. The reason for this is that the surface which is selective for the formation of maleic anhydride is the (0 2 0) plane. The thickness of the (2 0 4) plane is only an indicative of the mean length at the (2 0 4) face, while the (0 2 0) plane thickness represents the actual thickness. Hence, the exposure of the (0 2 0) plane would be of great significance in the improvement of the catalytic performance of the VPOs catalyst (Taufiq Yap et al., 2007).

Table 4.2: Comparison of the crystallite size from the conventional method and the microwave method

Catalyst	Crystallized size of the (0 2 0) plane obtained via conventional method[a] (Å)	Crystallized size of the (0 2 0) plane obtained via microwave method (Å)	Crystallized size of the (2 0 4) plane obtained via conventional method[a] (Å)	Crystallized size of the (2 0 4) plane obtained via microwave method (Å)
Bulk	108.28	72.337	209.37	109.437
Bismuth 1 %	149.21	81.402	132.79	75.066
Bismuth 3 %	187.78	87.838	114.41	56.388
Bismuth 5 %	118.40	126.683	44.02	55.023

[a] Obtained from Leong et al., (Catalysis Today, 164, 341-346, 2011),

4.3 Brunauer-Emmett-Teller (BET) Analysis

The surface areas of the catalyst are as follows: 17.5410 m^2g^{-1} for VPOs-Ba5,Bi1; 16.5124 m^2g^{-1} for VPOs-Ba5,Bi3 and 15.127 m^2g^{-1} for VPOs-Ba5,Bi5. All of which is larger than the surface area of the bulk catalyst, 12.6919 m^2g^{-1} for VPOs-Ba5 (Table 4.3). This suggests that the addition of bismuth had increased the surface area by intercalating into the VPOs structure and altering the development of the basal (1 0 0) plane structure (Leong et al., 2011).

Table 4.3: BET surface area analyst of the VPOs catalyst

Catalyst	Specific surface area (m^2g^{-1})
VPOs-Ba5	12.6919
VPOs-Ba5,Bi1	17.5410
VPOs-Ba5,Bi3	16.5124
VPOs-Ba5,Bi5	15.1270

As can be seen in the table above, increasing the bismuth addition decreases the surface area. The narrow pores are plugged and uniformly covered with the dopants causing the narrow pores to be no longer accessible for nitrogen molecules, which lead to a decrease in total surface area.

All the catalyst produced showed smaller surface area when compared with the catalyst produced via the conventional method (Table 4.4). The other factors influencing the surface area are such as catalyst porosity, the amount of platelets formed in the VPOs crystalline structure and the degree of isolation of the platelets.

Table 4.4: Comparison of the surface area from the conventional method and the microwave method obtained with bismuth addition

Catalyst	Conventional method[a] (m^2g^{-1})	Microwave irradiation (m^2g^{-1})
Bulk	19	12.69
With Bismuth 1 %	29	17.54
With Bismuth 3 %	22	16.51
With Bismuth 5 %	21	15.13

[a] Obtained from Leong et al., (Catalysis Today, 164, 341-346, 2011),

According to Zazhigalov et al., (1996), addition of barium decreases the surface area. Since the catalyst is bimetallic doped which consists of both bismuth and barium, the addition of the other dopant should also be taken into account. Since catalyst with higher surface area would have more split $(VO)_2P_2O_7$ while catalyst with lower surface area would have higher crystallite size. This is proven with the XRD result mentioned earlier, as the bismuth addition increased, the crystallite size in (0 2 0) plane increased, thus reducing the surface area.

All the synthesized VPOs catalyst have showed similar adsorption desorption graphs, indicating that the addition of dopants does not affect the type of isotherm. From the isotherm graphs shown in Figure 4.4 till Figure 4.7, all the VPOs catalyst belongs to Type IV isotherm, shown in Figure 4.3 which represents the mesoporous adsorbents that arises from strong liquid-solid interaction (Kruk et al., 1999).

Mesoporous are the result of major defects in the structure of the solid. They give rise to the phenomenon of capillary condensation which is observed by the existence of an inherent hysteresis loop as there are differences in the pore filling and emptying process. The pore size is bigger than 2 nm but smaller than 50 nm (Kruk et al., 1999).

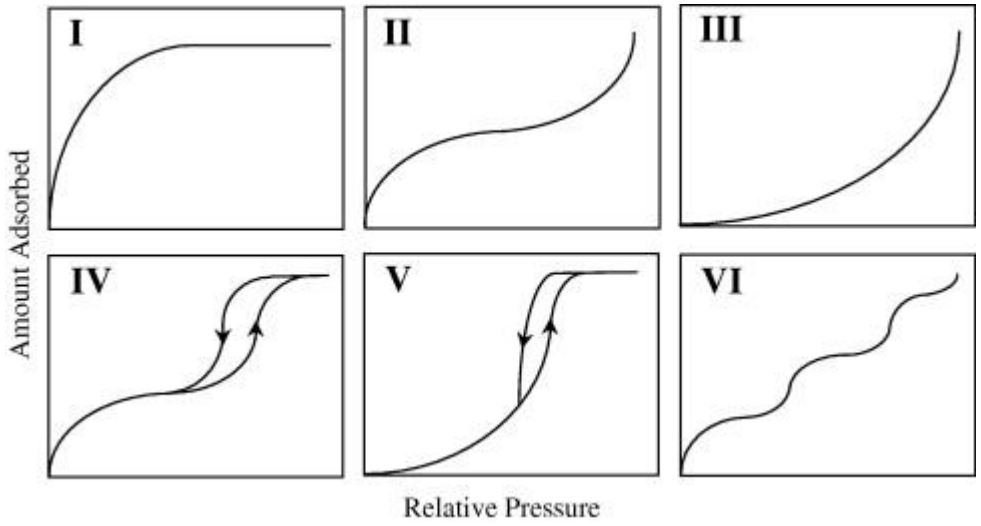

Figure 4.3: IUPAC classification for isotherms

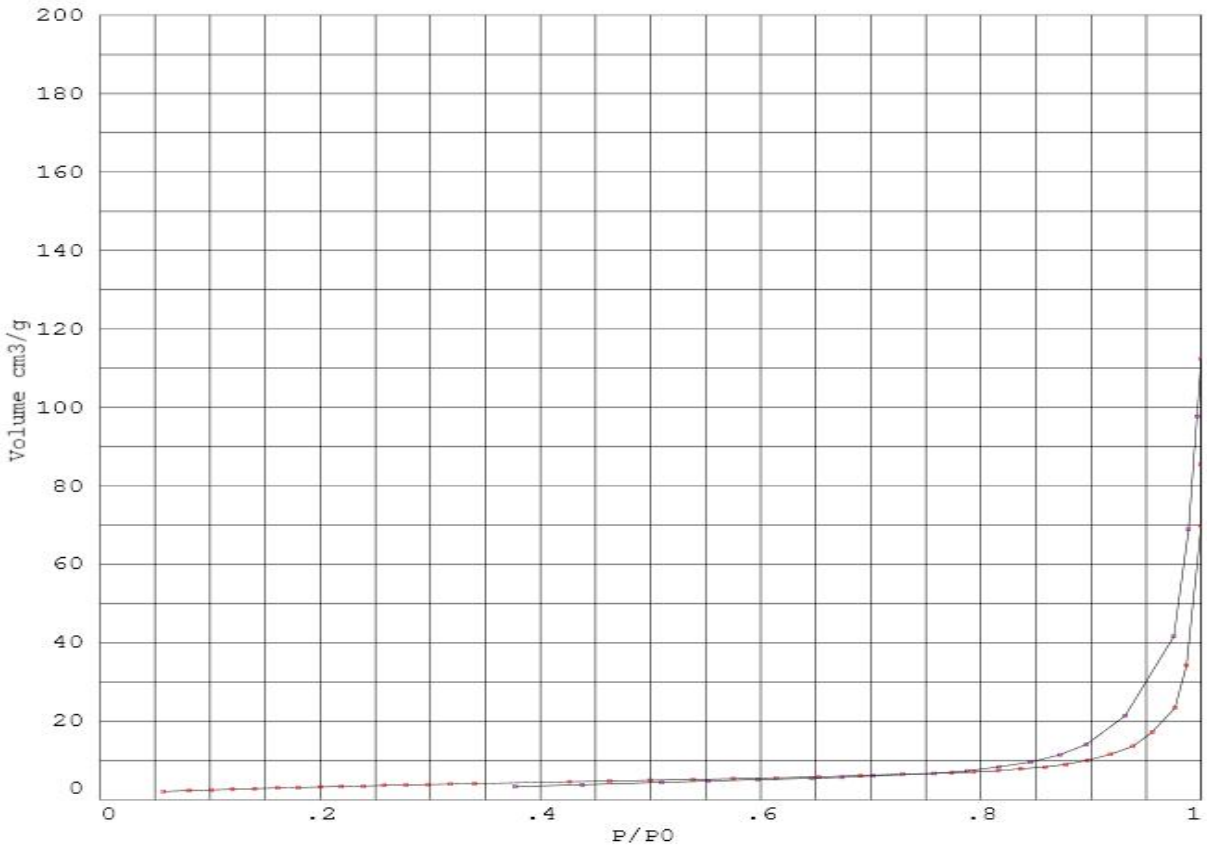

Figure 4.4: Adsorption Desorption Isotherm for VPOs-Ba5

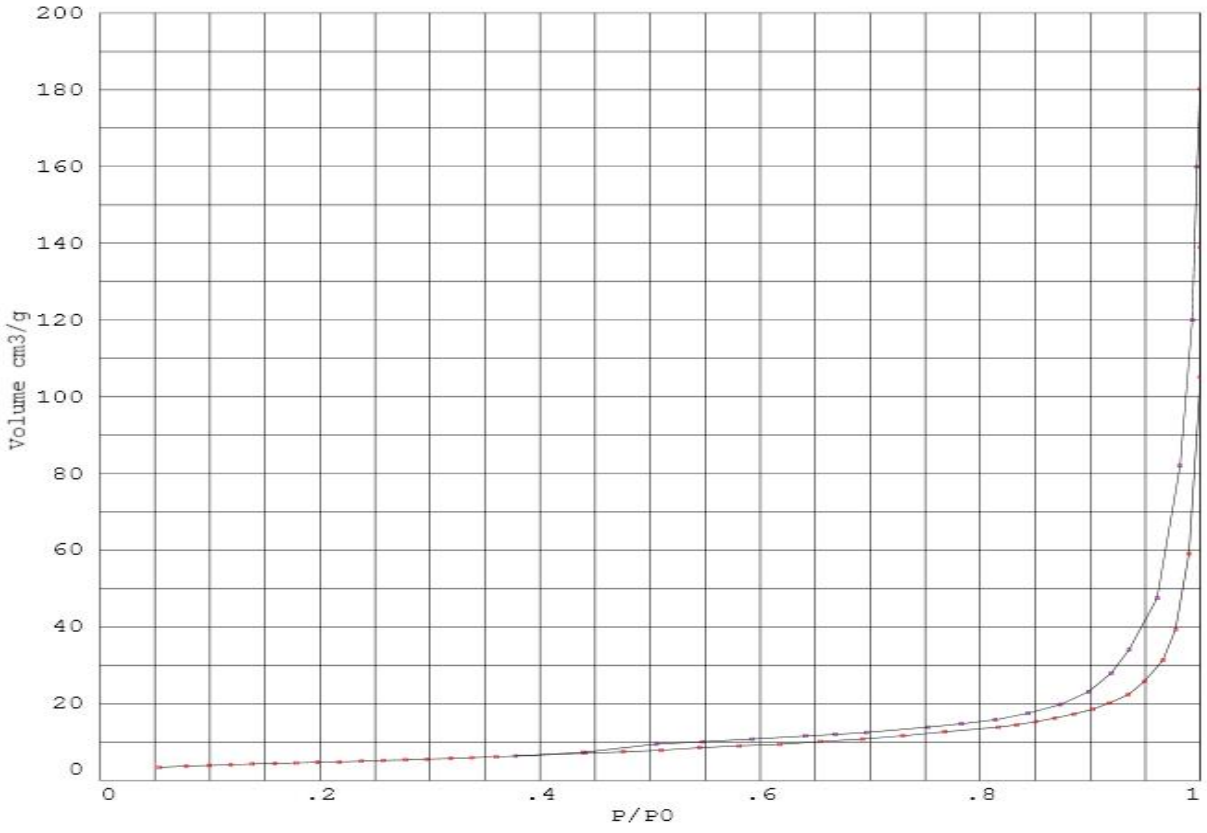

Figure 4.5: Adsorption Desorption Isotherm for VPOs-Ba5,Bi1

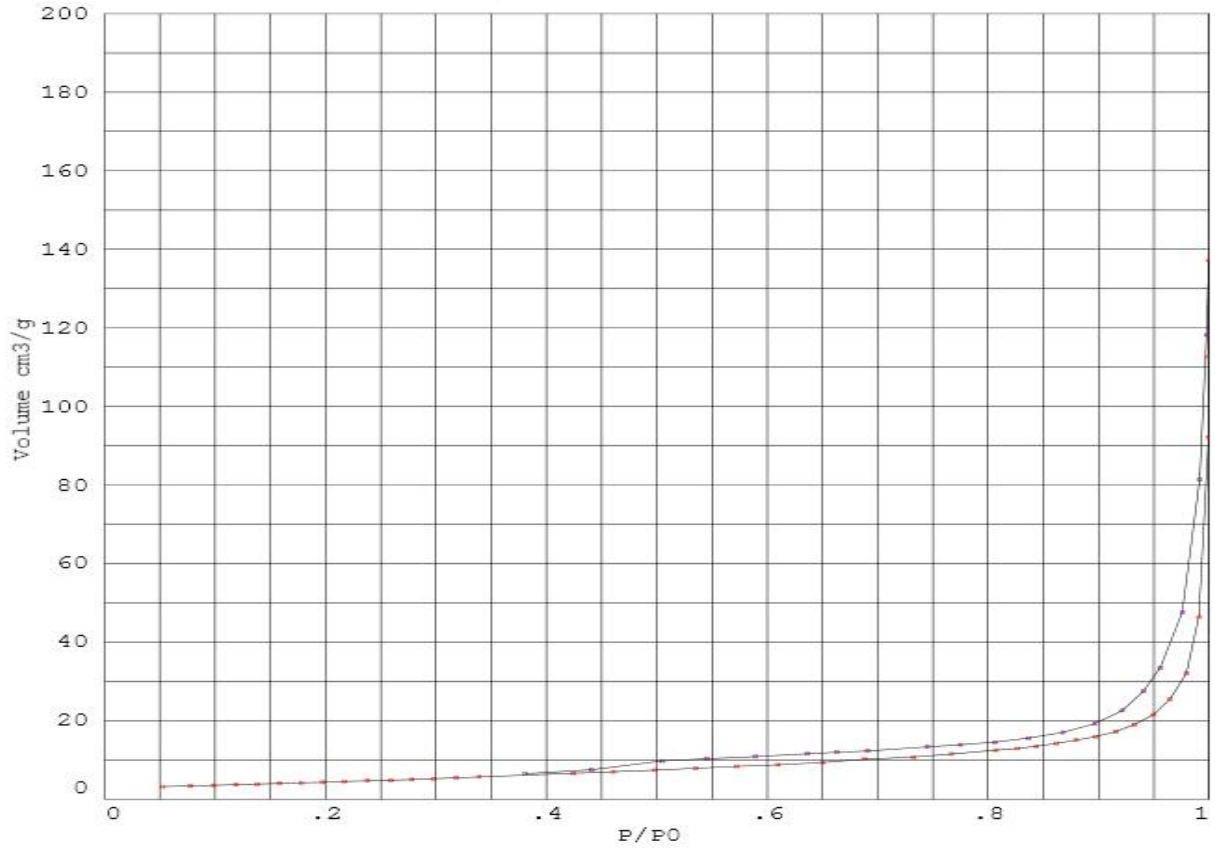

Figure 4.6: Adsorption Desorption Isotherm for VPOs-Ba5,Bi3

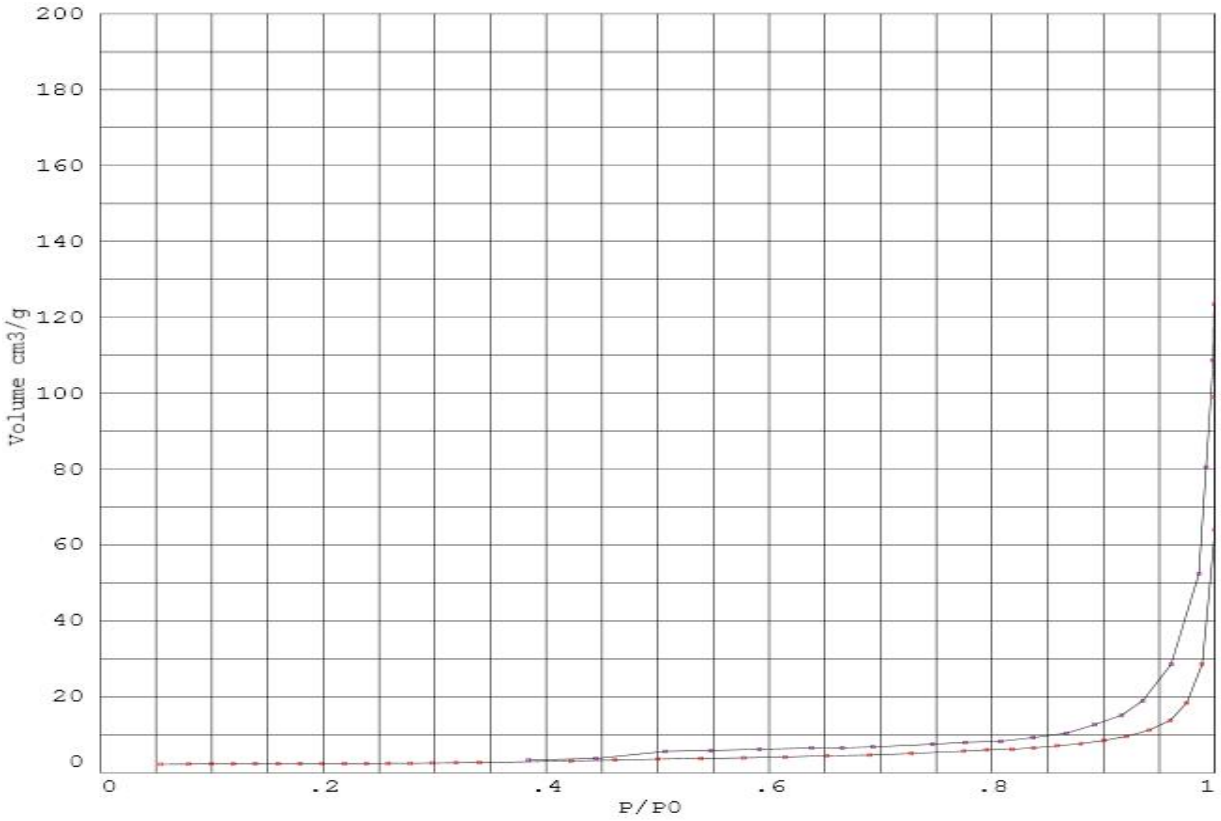

Figure 4.7: Adsorption Desorption Isotherm for VPOs-Ba5,Bi5

4.4 Scanning Electron Microscopy (SEM) Analysis

The surface morphology of all the catalysts are shown in the following figures obtained from the SEM. These catalysts showed similar structure, consisting of different sizes of platelets like crystals which are agglomerated into a layered cluster. Where the platelet like crystals are comprised of agglomerates of $(VO)_2P_2O_7$ platelets, which are exposing the (1 0 0) crystal plane. Figure 4.8 till Figure 4.11 shows the micrographs of the catalyst at different magnifications, whereby images denoted as (A) had been magnified 500 times while (B) had 5000 been magnified 5000 times.

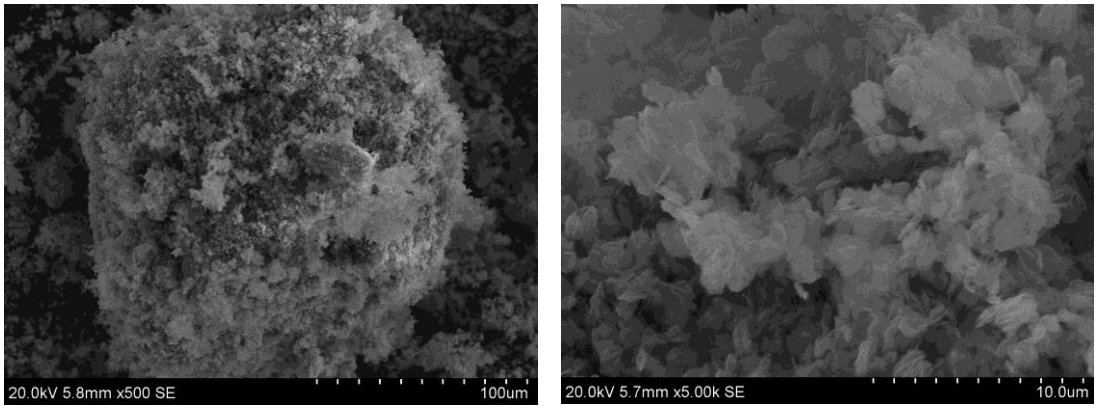

(A) (B)

Figure 4.8: SEM Micrograph for VPOs-Ba5: (A) x 500 (B) x 5000

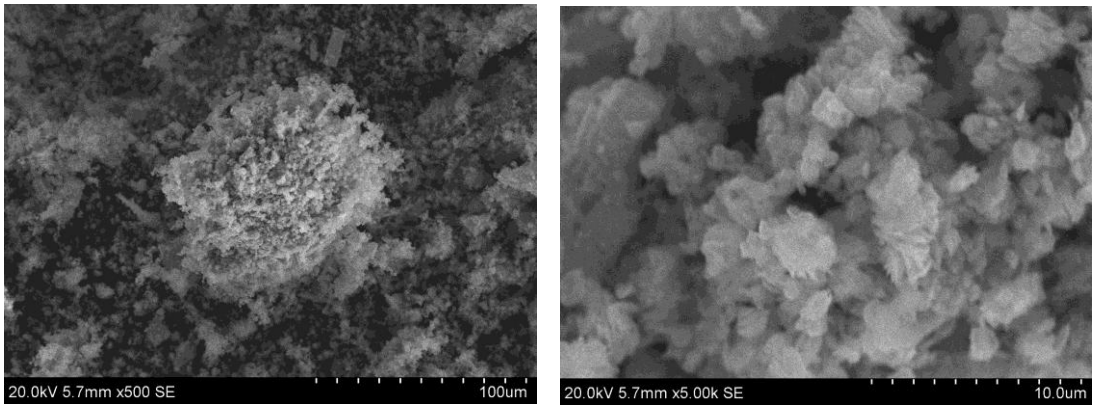

(A) (B)

Figure 4.9: SEM Micrograph for VPOs-Ba5,Bi1: (A) x 500 (B) x 5000

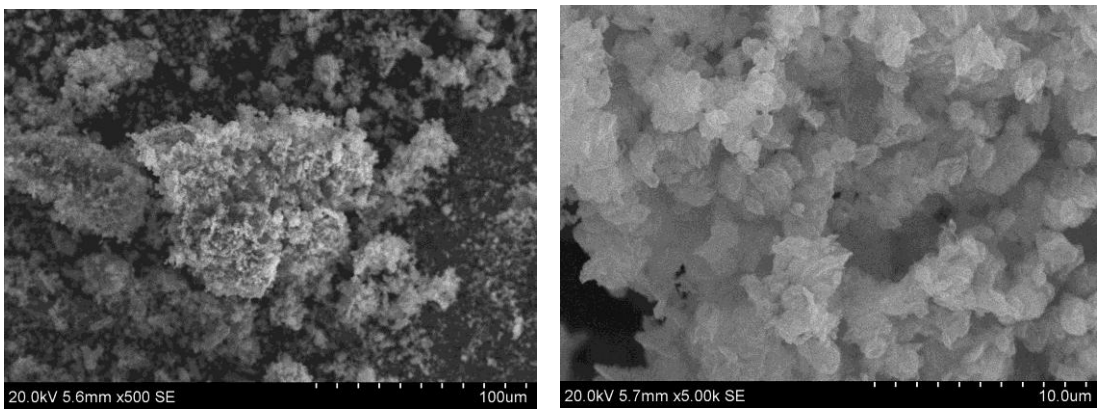

(A) (B)

Figure 4.10: SEM Micrograph for VPOs-Ba5,Bi3: (A) x 500 (B) x 5000

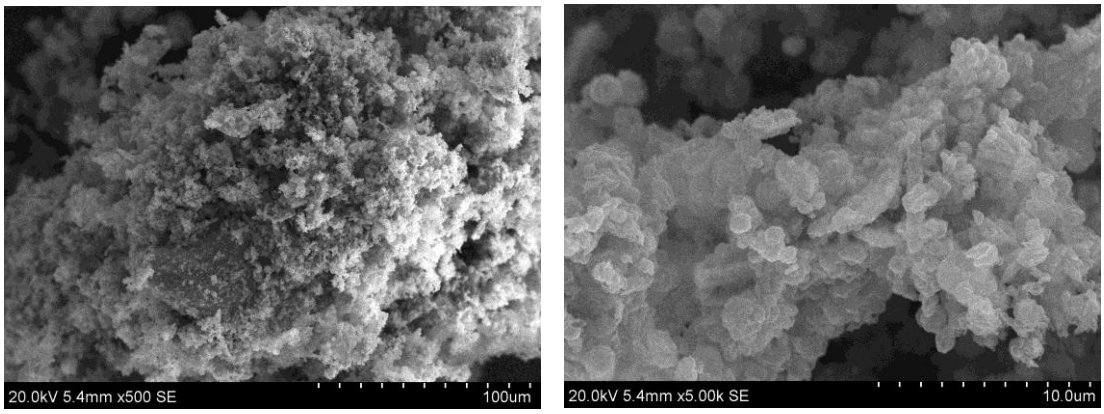

(A) (B)

Figure 4.11: SEM Micrograph for VPOs-Ba5,Bi5: (A) x 500 (B) x 5000

As the bismuth addition is increased the size of the cluster increases, which supports the XRD result obtained for increasing crystallite size in the (0 2 0) plane with addition of bismuth. It also had resulted in more layered platelet like crystals which stacks together that result in lower surface area. This is in agreement with the BET result, as the percentage of bismuth addition increased, the specific surface area decreases.

The agglomerated cluster of the bismuth doped catalyst is smaller than the bulk catalyst, resulting in higher specific surface area compared to the bulk catalyst. This is due to the addition of bismuth, which had provided sufficient shear force that allowed the crystal platelets to slide away from one another, thereby exposing more surface plane (Kiely et al., 1995).

Taking a closer look at the catalyst, it is observed that it appeared to have blocky type of rectangular shaped crystallites, which were assigned to the presence of the β-$VOPO_4$ phase. This particular type of crystallite structure was discerned to match with the structure of β-$VOPO_4$ pure standards, which was adopted by Kiely and his co-workers in a different approach to study and characterize all VPO phases. Hence, the micrograph results confirm the presence of the V^{5+} phase in the catalyst that is observed from the XRD analysis which is attributed to higher selectivity.

Table 4.5 summarizes the important information regarding the phases in VPOs catalyst, such as crystallography and morphology based on pure standards. Figure 4.12 shows the images described in Table 4.5.

Table 4.5: Crystallographic and Morphological Data on Standard Phases

Compounds	Crystal Group[a]	Morphology[a]
$VOHPO_4 \cdot 0.5H_2O$	Orthorhombic	Highly dependent on precise preparation route
α_1-$VOPO_4$	Tetragonal	Featureless platelets with (001) normal Figure 4.12 (A)
α_{11}-$VOPO_4$	Tetragonal	Platelets with distinctive surface structure Figure 4.12 (B)
β-$VOPO_4$	Orthorhombic	Dense agglomerates of randomly oriented angular platelets Figure 4.12 (C)
γ-$VOPO_4$	Monoclinic	Dense agglomerates of platelets showing "desert rosette" type structure Figure 4.12 (D)
δ-$VOPO_4$	Orthorhombic	Random cluster of irregular platelets frequently exhibiting parallel slashes Figure 4.12 (E)
$(VO)_2P_2O_7$	Orthorhombic	Facetted needle like crystals if basal (100) plane is often exposed Figure 4.12 (F)

[a] Obtained from Kiely et al., (Journal of Catalysis, 162, 31-47, 1996),

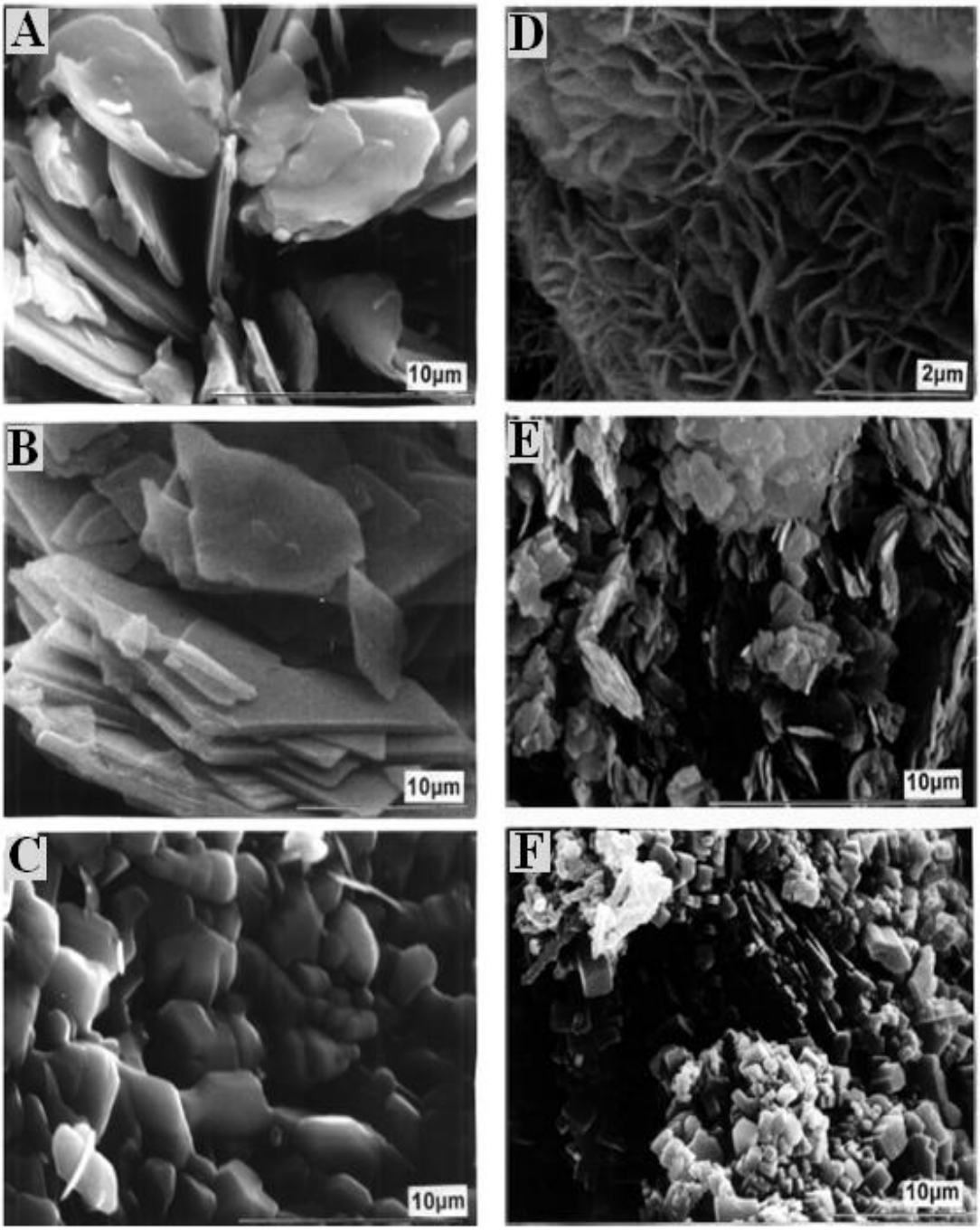

Figure 4.12: Representative SEM micrographs from Standard Phases:

(A): α_1-$VOPO_4$ (B): α_{11}-$VOPO_4$ (C): β-$VOPO_4$ (D): γ-$VOPO_4$ (E): δ-$VOPO_4$ (F): $(VO)_2P_2O_7$

In this research, the dopants are added to the sesquihydrate precursor implying physical mixing. During the physical mixing, these crystal platelets are broken into smaller pieces thus decreasing the exposure to the surface plane. These smaller pieces are unstable and have high tendency to agglomerate, causing a decrease in the surface area of the catalyst.

Rownaghi et al., (2010), found that microwave irradiation synthesis was highly dependent on the type of reducing agent. Solvents with different physical and chemical properties can influence the solubility, reactivity and diffusion behaviour of the reactants. In particular, the polarity and coordinating ability of the solvent can change the morphology and the crystallization behaviour of the final products.

When compared the surface area obtained via microwave irradiation method implying different types of reducing agent, the catalyst prepared using isobutanol yields higher surface area compared to other reducing agents such as pentanol, heptanol and decanol. The presence of lengthy alkyl chain dramatically increases the hydrophobic nature, leading to a lower diffusion rate of ions in the solvent and finally to the formation of smaller particles. These smaller particles tend to agglomerate and leading to smaller surface area (Rownaghi et al., 2010).

4.5 Energy Dispersive X-ray (EDX) Analysis

Accuracy of the EDX could be affected by a few factors. Elements having overlapping peaks are one of the reasons. Besides that, the energy of the x-ray emitted by the excited atom also plays an important role. For the x-ray emitted to be detected and measured, it depends on the energy of the x-ray as well as the amount and density of the material it has to pass through. These can result in reduced accuracy in inhomogeneous and rough samples.

Thus, to minimize the inaccuracy of the result obtained, 5 points are selected and it is averaged to obtain the P_{avg} and V_{avg}, where the latter is divided with the P_{avg} to obtain the average P/V ratio. As some point might have a far deviated value from others, only those points that yield closer value are taken into account, while outliers are omitted.

Table 4.6: P/V ratio obtained from EDX

Catalyst	P_{avg} (at %)	V_{avg} (at %)	Average P/V
VPOs-Ba5	25.103	22.873	1.097
VPOs-Ba5,Bi1	24.781	22.840	1.085
VPOs-Ba5,Bi3	23.776	22.796	1.043
VPOs-Ba5,Bi5	23.346	22.761	1.026

It is seen that addition bismuth decreases the average P/V, which is a result from the lower phosphorus content. According to Guliants et al., (2005), that the optimal catalyst composition is characterized by slight excess of phosphate, since it helps to stabilize the V^{4+} oxidation and prevent the over oxidation of $(VO)_2P_2O_7$ to $VOPO_4$. Hence, the lower phosphorus content results in more oxidize V^{4+} phase, which is supported by the $VOPO_4$ phases found in the XRD analysis.

Possible reasons for lower phosphorus detection might be due to the inhibition of the surface enrichment of phosphorus by the microwave irradiation leading to lesser phosphorus detected on the catalyst surface. Moreover, since EDX is only a surface technique, penetration of the catalyst surface is only up to a few microns.

4.6 Redox Titration Analysis

The obtained average vanadium oxidation number is tabulated in Table 4.7.

Table 4.7: Average oxidation number of vanadium

Catalyst	V^{4+} (%)	V^{5+} (%)	V_{av}
VPOs-Ba5	63.49	36.51	4.4286
VPOs-Ba5,Bi1	39.92	60.08	4.6008
VPOs-Ba5,Bi3	34.91	65.09	4.6509
VPOs-Ba5,Bi5	30.20	69.80	4.6980

Redox titration result of more than 4.0 for all the samples shows that the samples consists of both V^{4+} and V^{5+} phases. Percentage of V^{4+} decreases, while the percentage of V^{5+} increase as the percentage of bismuth addition is increased. The V_{av} obtained is getting further away from 4.0, indicating that more V^{5+} phases are formed as the addition of bismuth increased.

This is supported by the V^{5+} peaks found in the XRD, getting more intense as the bismuth addition is increased as well as the SEM result, indicating the blocky crystallite structure which represents the β-$VOPO_4$ phase belonging to the V^{5+}. EDX analysis also supports the result obtained since the reduction in the P/V ratio signifies that lesser phosphorus content in the catalyst and the V^{4+} phases are oxidized to V^{5+} phases.

Table 4.8: Comparison of the V_{AV} from the conventional method and the microwave method obtained with bismuth addition

Catalyst	Conventional method[a]	Microwave irradiation
Bulk	4.0419	4.4286
With Bismuth 1 %	4.4581	4.6008
With Bismuth 3 %	4.4120	4.6509
With Bismuth 5 %	4.5026	4.6980

[a] Obtained from Leong et al., (Catalysis Today, 164, 341-346, 2011),

From the comparison shown in Table 4.8 above, is it observed that Leong et al., (2011) also had obtained similar findings for addition of bismuth. When compared with the values obtained from the conventional method, V_{av} from microwave irradiation technique is generally higher. This is in agreement with Taufiq Yap et al., (2007) since microwave irradiation increases the average oxidation number by inducing the presence of higher amount of V^{5+} phase.

The increment in the V^{5+} as the bismuth addition increases shows that the catalyst is more selective rather than active. This is agreeable with the findings of Guliants and Carreon, (2005) since the VPOs catalyst characterized with a high V^{5+} content have higher selectivity with lower activity.

Zazhigalov et al., (1996) found that addition of alkali and alkaline earth metals to the VPOs catalyst causes an increase in the surface P/V ratio due to the enrichment of the surface with phosphorus that occurs at the expense of outward diffusion of over stoichiometric phosphorus though the pellet.

This rise of phosphorus concentration on the surface is accompanied by simultaneous enrichment of the surface in oxygen and increase in oxygen basicity. Such changes in the surface composition lead to corresponding changes of acidic properties of the catalysts. The amount of adsorbed base increases with the rise of P/V ratio (Zazhigalov et al., 1996).

The selectivity towards maleic anhydride is dependent on the amount of acidic centres at the surface catalyst. At low acidity of the surface, desorption of adsorbed acid like products of the reaction is hindered and further oxidation occurs with CO_X formation. On the other hand, high acidity of the surface does not favour the adsorption of intermediates with acidic properties (Zazhigalov et al., 1996).

It can thus be concluded that addition of alkali and alkaline earth metals to VPOs composition allow changes to both activity and selectivity of the catalyst. An increase the selectivity towards maleic anhydride is observed after the introduction of barium (Zazhigalov et al., 1996).

4.7 Temperature Program Reduction (TPR)

TPR in H_2 analyses were used to investigate the redox properties of the catalyst. Additional information such as nature and the oxidising species available from the catalysts could be obtained as well. Figure 4.13 shows the TPR profile of the catalysts in H_2/Ar stream (5.23 % H2 in Ar, 1000 Pa, and 25 cm^3 min^{-1}) using a fresh sample of catalyst and raising the temperature from ambient to 1273 K at 10 K min^{-1} in that stream. Table 4.10 lists the peaks maximum temperatures, reduction activation energy, the amount of oxygen in each peak, the ratio of V^{5+}/V^{4+} and V^{4+}/V

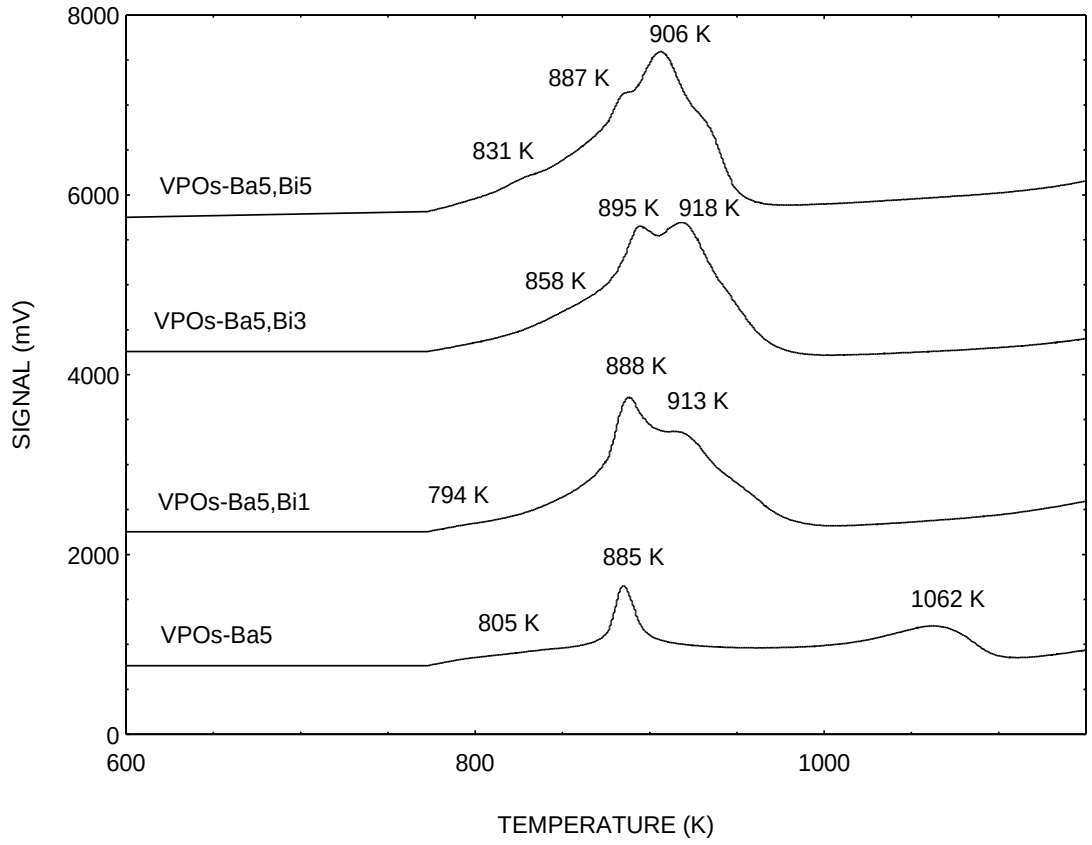

Figure 4.13: TPR Profiles for Different Percentage of Bimetallic Dopants

A few important points were observed in the TPR profiles. All the catalyst gave three peak maxima in the reduction by H_2. The first two peaks corresponded to the reduction of V^{5+} phase, whereas the third peak was assigned to the removal of the lattice oxygen from the active V^{4+} phase. The peak attributed to V^{4+} was associated with the removal of O^- anion and the peak from V^{5+} was related to the oxygen species of O^{2-}. For the bulk catalyst, the reduction of V^{4+} appeared to be the major peak and this concludes that V^{4+} is the predominant species in the catalyst as shown in the redox titration results, where 63.49 % of V^{4+} was obtained (Leong et al., 2011).

Table 4.9: Summary of TPR Analysis

Catalyst	Peak	T_m (K)	Reduction activation energy, E_r (KJ mol^{-1})	Amount of oxygen removed (mol g^{-1})	Amount of oxygen removed (atom g^{-1})	Ratio for oxygen removal of V^{5+}/V^{4+}	Ratio for oxygen removal of V^{4+}/V^{5+}.
Ba5 %	1	805	123.764	7.957×10^{-5}	4.790×10^{19}	0.476	2.101
	2	885	136.064	3.618×10^{-4}	2.178×10^{20}		
	3	1062	163.276	9.276×10^{-4}	5.584×10^{20}		
			Total	**1.369×10^{-3}**	**8.241×10^{20}**		
Ba5 %, Bi1 %	1	794	122.073	1.870×10^{-3}	1.126×10^{21}	1.164	0.859
	2	888	136.525	2.328×10^{-3}	1.401×10^{21}		
	3	913	140.366	3.606×10^{-3}	2.171×10^{21}		
			Total	**7.799×10^{-3}**	**4.701×10^{21}**		
Ba5 %, Bi3 %	1	858	132.375	6.722×10^{-4}	4.047×10^{20}	1.212	0.825
	2	895	137.601	2.105×10^{-3}	1.268×10^{21}		
	3	918	141.138	2.291×10^{-3}	1.379×10^{21}		
			Total	**5.068×10^{-3}**	**3.052×10^{21}**		
Ba5 %, Bi5 %	1	831	128.209	1.899×10^{-3}	1.143×10^{21}	1.342	0.745
	2	887	136.371	2.466×10^{-3}	1.485×10^{21}		
	3	906	139.293	3.252×10^{-3}	1.958×10^{21}		
			Total	**7.617×10^{-3}**	**4.586×10^{21}**		

By increasing percentage of bismuth with the introduction of barium into the VPOs catalyst, the reduction patterns have changed significantly with the reduction of V^{5+} species appeared to be predominant, whereas the reduction peak of V^{4+} was reduced. The incorporation of elements which can easily donate electrons to the structure of vanadyl phosphate increases the effective negative charge on the oxygen which in return increases the basic property of the catalyst (Haber et al., 1997).

As a consequence, the amount of adsorbed CO_2 molecules on the catalyst surface increases, which is also an effect of decrease in the binding energy of the O1s-electrons that is accompanied by the lowering of the reduction temperature. This effect may be due to either the accelerated activation of hydrogen by more basic oxygen or to decrease of the lattice energy related to the substitution of low valent cations into the crystal lattice (Haber et al., 1997).

Figure 4.13 and 4.14 shows the graph correlation for the ratio for oxygen removed with percentage of bismuth added. As can be seen in Figure 4.13, addition of bismuth greatly increases the ratio of V^{5+}/V^{4+}, indicating that more V^{5+} phase are being removed compared to V^{4+} phase. Vice versa, the removal of V^{4+} phase reduced dramatically as more bismuth is incorporated in the VPOs catalyst.

Highest ratio of V^{5+}/V^{4+} is obtained from the VPOs-Ba5,Bi5, which also gives the lowest V^{4+}/ V^{5+}. Higher oxygen species associated to V^{5+} phase removal suggest that these catalysts will show a poor activity but a higher selectivity, which favour the formation of maleic anhydride. This is supported by all the previous analysis which yielded higher tendency towards selectivity rather than activity, due to the presence of more V^{5+} comparing to V^{4+}

Thus, it can be concluded that TPR in H_2 analyses results had indicated that the addition of increasing amounts of Bi promoter would lead to the enhancement of the amount of oxygen species associated with the V^{5+} with slight effect on the amount of oxygen removed from the V^{4+} phase.

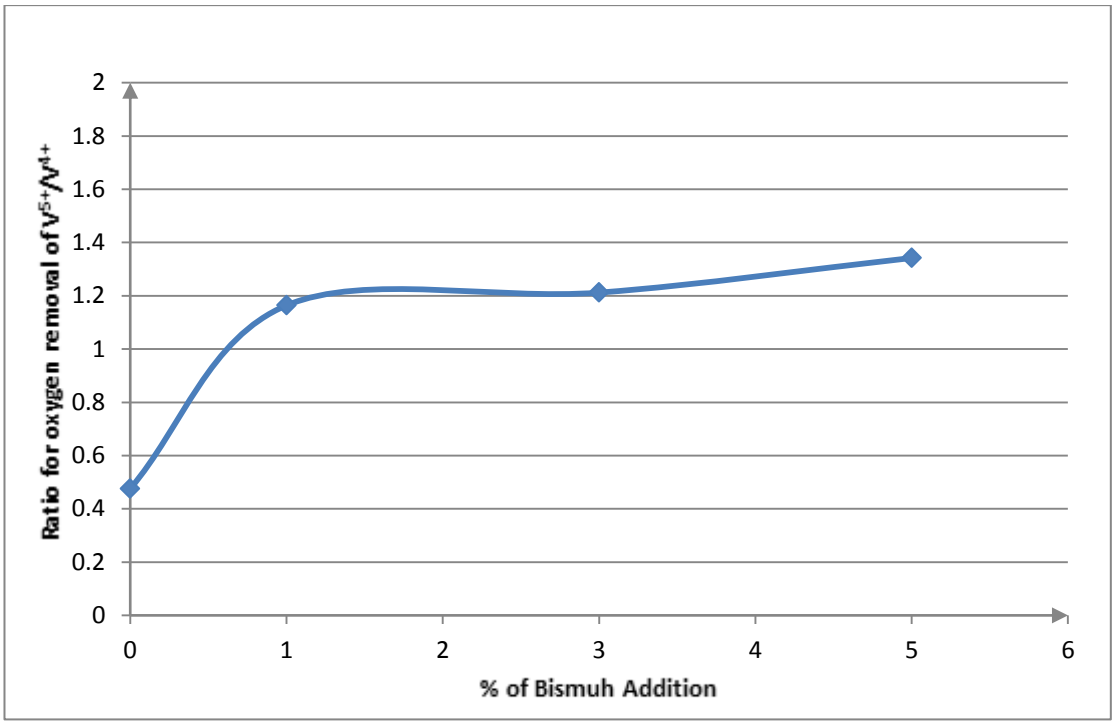

Figure 4.14: Correlation of Ratio for oxygen removal of V^{5+}/V^{4+} with % of Bismuth addition

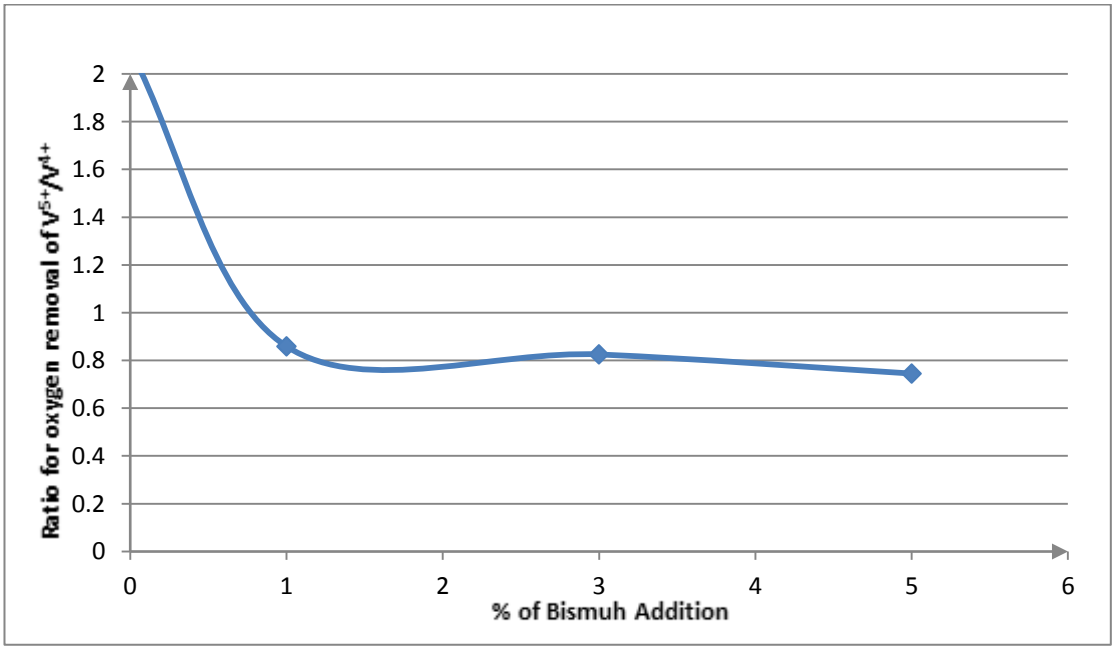

Figure 4.15: Correlation of Ratio for oxygen removal of V^{4+}/V^{5+} with % of Bismuth addition

CHAPTER 5

CONCLUSION AND RECOMMENDATION

5.1 Conclusion

The catalysts obtained were denoted as VPOs-Ba5, VPOs-Ba5,Bi1, VPOs-Ba5,Bi3 and VPOs-Ba5,Bi5. The effect of bimetallic dopant prepared via a microwave irradiation technique for the first stage and reflux technique for the second stage were studied.

Generally all synthesized catalyst exhibited similar crystallite sizes and surface morphologies as seen in the XRD and SEM analysis respectively. From the BET analysis, VPOs-Ba5,Bi1 yields the highest surface area of 17.54 m^2g^{-1}, with the bulk having the lowest surface area of 12.69 m^2g^{-1}. As for EDX analysis, the bulk yields the best result, since there should be a slight excess of phosphate for an optimal catalyst composition. However, VPOs-Ba5,Bi1 also yields an acceptable result since the difference between the two is only 0.012.

Highest V_{AV} is given by VPOs-Ba5,Bi5, which indicates a rather selective catalyst, while the bulk yields the lowest V_{AV}. The difference between the highest V_{AV} and obtained from VPOs-Ba5,Bi1 is within an acceptable range of 0.0972 indicating that the latter catalyst is slightly lower in selectivity compared to the VPOs-Ba5,Bi5 but better in terms of activity.

TPR analysis shows that VPOs-Ba5,Bi1 has the highest amount of total oxygen removed, which is 4.701 x 10^{21} atom g^{-1} while the bulk yields the lowest oxygen removed. Hence, an optimal catalyst for the research would be VPOs-Ba5,Bi1 as it has a better compromise between selectivity and activity as an optimal catalyst.

In conclusion:

1. All catalyst exhibited good crystalline with characteristic peaks of vanadyl pyrophosphate phase and their surface morphologies were found to be in platelet like crystals agglomerated as clusters.
2. Bismuth was found to be a good structural promoter as it increased the specific surface area of the VPOs catalyst,
3. Bismuth promoted catalyst gave a better catalytic performance with higher selectivity which is shown in TPR analysis with higher amount of lattice oxygen removed associated to the ratio of V^{5+}/V^{4+}.

5.2 Recommendations

For further research:

1. Catalyst produced should be tested using the catalytic reactor which would yield the selectivity of the catalyst towards maleic anhydride formation and activity toward *n*-butane conversion. These data as crucial as they play an important role in determining the optimal catalyst.
2. Various dopants can be added so that the effect of doping towards the physical, chemical, reactivity and catalytic properties of the doped VPOs catalyst can be studied.
3. Catalyst should be prepared via microwave irradiation for both first and second stage implying the sesquihydrate route and the result obtained compared between organic and hemihydrate route to distinguish a better and newer way of producing catalyst.

REFERENCES

Bartholomew, C. H., & Farrauto, R. J. (2005). *Fundamentals of industrial catalytic processes (2nd Ed.)*. Wiley-Interscience: John Wiley & Sons Inc.

Bond, G. C. (1987). *Heterogeneous catalysis: Principles and applications, 2nd ed*. London: Oxford University Press.

Boss, C. B., & Fredeen, K. J. (1997). *Concepts instrumentation and techniques in inductively coupled plasma optical emission spectrometry (2nd Ed.).* United States of America: Perkin Elmer Corporation.

Centi, G., & Trifiro, F. (1990). *New developments in selective oxidation.* Elsevier Science Publication.

Centi, G., Trifiro, F., Ebner, J. R., & Franchetti, V. M. (1988). Mechanistic aspects of maleic anhydride synthesis from C_4 hydrocarbon over phosphorus vanadium oxide. *Chem. Rev*., 88(1), 55-80.

ChemSystems. (2009, April). *Maleic anhydride*. Retrieved from http://www.chemsystems.com/reports/search/docs/abstracts/0708_8_abs.pdf on 18th August 2011.

Cheng, W. H. (1996). Effect of composition of promoted VPO catalyst on selectivity oxidation of *n*-butane to maleic anhydride. *Applied Catalysis A: General*, 147(1), 55-57.

Chorkendorff, I., & Niemantsverdriet, J. W. (2003). *Concept of modern catalysis and kinetics*. Wiley-Interscience: John Wiley & Sons Inc.

Datta, A., Agarwal, M., & Dasgupta, S. (2002). Novel vanadium phosphate phases as catalyst for selective oxidation. *Proc. Indian Acad. Sci*., 114(4), 379-390.

Daxiang, W., & Barteau, M. A. (2002). Oxidation kinetics of partially reduced vanadyl pyrophosphate catalyst. *Applied Catalysis A: General-Elsevier*., 223(1-2), 205-214.

Ebner, J. R., & Thompson, M. R. (1993). An active site hypothesis for well crystallized vanadium phosphorus oxide catalyst systems. *Catalysis Today*, 16(51). 51-60.

Felthouse, T. R., Burnett, J. C., Horrell, B., Mummey, M. J., & Kou, Y. J. (2001). *Maleic anhydride, maleic acid and fumaric acid*. Retrieved from http://www.southalabama.edu/chemistry/barletta/felthouse.pdf on 18th August 2011.

Guliants, V. V., & Carreon, M. A. (2005). Vanadium phosphorus oxide: Fundamentals of *n*-Butane oxidation to synthesis of new phases. *The Royal Society of Chemistry Publishing*, 55(3), 13-15.

Haber, J. (1994). Catalysis: Where science and industry meet. *Pure & Appl. Chem*., 66(8), 1597-1620.

Haber, J., Zazhigalov, V. A., Stoch, J., Bogutskaya, L. V. & Batcherikova, I. V. (1997). Mechanochemistry: the activation method of VPO catalyst for *n*-butane partial oxidation. *Catalysis Today*, 33, 39-47.

Huang, X. F., Chen, B. H., Liu, B. J., Silveston, P. L., & Li, C. Y. (2002). *Reoxidation kinetics of a VPO catalyst*. Catalysis Today, 74(1-2), 121-130.

Kiely, C. J., Burrows, A., Sajip, S., Hutchings, G. J., Sananes, M. T., Yuel, A. & Volta, J. C. (1996). Characterization of variations vanadium phosphate catalyst microstructure with preparation route. *Journal of Catalysis*, 162, 31-47.

Kruk, E. N., Jarry, K. C., William, N. W. & Jessi, B. A. (1999). Isotherms of the VPOs synthesized catalyst. *Catalysis Today*, 193, 204-210.

Leong, L. K., Chin, K. S. & Taufiq Yap, Y. H. (2011). The effect of bi promoter on vanadium phosphate catalysis synthesized via sesquihydrate route. *Catalysis Today*, 164, 341-346.

Leong, L. K., Chin, K. S. & Taufiq Yap, Y. H. (2012). Effect of varying reflux duration on the phyico-chemical and catalytic performance of vanadium phosphate catalyst synthesized via vanadyl hydrogen phosphate sesquihydrate. *Applied Catalysis A: General*, 415-416, 53-58.

Masilo, N. (2009). *n-butane activation over Ruthenium and Iron promoted catalyst*. (Unpublished Master Research Project). University of KwaZulu-Natal.

Morishige, H., Tamaki, J., Miara, N. & Yamazoe, N. (1990). *Chem. Lett.*1513.

Niwa, M. & Murakami, Y. (1982). Reaction mechanism of ammoxidation of toluene IV oxidation state of vanadium oxide and its reactivity for toluene oxidation. *Journal Catalysis*, 76, 9-16.

Rownaghi, A. A., Taufiq Yap, Y. H. & Rezaei, F. (2010). Innovative process for the synthesis of vanadyl pyrophosphate as a highly selective catalyst for *n*-butane oxidation. *Chemical Engineering Journal*, 165, 328-335.

Ruitenbeek, M. (1998). Effects of silica and titania supports on the catalytic performance of V-P-O catalysts. *Elsevier Science Publication*, 118, 52.

Shimadzu Corporation. (2007). *Shimadzu x-ray diffractometer*. Retrieved from http://www.shimadzu.com/an/elemental/xrd/xrd6000.pdf on 21st August 2011.

Slindard, W., & Baylis, A. (1996). *Production of maleic anhydride*. Retrieved from http://www.che.cemr.wvu.edu/publications/projects/large_proj/maleic on 20th August 2011.

Taufiq-Yap, Y. H., Looi, M., Wong, Y., & Hussien, M. Z. (2001). Physico-chemical characterization of vanadium phosphorus-oxide catalyst prepared in organic and aqueous medium. *Jurnal Teknologi*, 34(C), 17-24.

Taufiq-Yap, Y. H., Leong, L. K., Hussien, M. Z., Irmawati, R., & Abd Hamid, S. B. (2004). Synthesis and characterization of vanadyl pyrophosphate catalyst via vanadyl hydrogen phosphate sesquihydrate precursor. *Catalysis Today*, 93-95, 715-722.

Taufiq-Yap, Y. H., Goh, C. K., Hutchings, G. J., Dummer, N., & Bartley, J. K. (2006). Effect of mechanochemical treatment to the vanadium phosphate catalysts derived from $VOPO_4 \cdot 2H_2O$. *Journal of Molecular Catalysis*, 260(1-2), 24-31.

Taufiq Yap, Y. H., Rownanghi. A. A., Hussien, M. Z. & Irmawati, R. (2007). Preparation of vanadium phosphate catalyst from $VOPO_4 \cdot 2H_2O$: Effect of microwave irradiation on morphology and catalytic property. *Catalyst Letter*, 119, 64-71.

Trifiro, F. (1998). The chemistry of oxidation catalyst based on mixed oxides. *Catalysis Today*, 41, 21-35.

Trivedi, B. C., & Culberston, B. M. (1982). *Maleic anhydride*. New York: Plenum Press.

Viswanathan. B., Sivasanker, S., & Ramasamy, A. V. (2002). *Catalysis: Principles & applications*. Narosa Publishing House.

World Petrochemicals. (2011). *Maleic anhydride*. Retrieved from http://chemical.ihs.com/WP/Public/Reports/ma/ on 22nd August 2011.

Zazhigalov, V. A., Haber, J., Stoch, J., Bacherikokva, I. V., Komashko, G. A., & Pyatnitskaya, A. I. (1996). *n*-Butane oxidationon V-P-O catalyst: Influence of alkali and alkaline-earth metals ions as additions. *Applied Catalysis A: General*, 33(1-3), 225-237.

APPENDICES

APPENDIX A: Volume of Distilled Water Used

1. Prepare the amount of water needed to be used

24ml H_2O/g V_2O_5 is required.

15g of V_2O_5 is used as a starting material

Thus, the volume of distilled water needed = 15g × (24ml H_2O/g Solid)

= 360 ml

APPENDIX B: Volume of 1-butanol Used

1. Determine the molecular weight of $VOPO_4 \cdot 2H_2O$

Molecular formula of vanadyl phosphate dihydrate = $VOPO_4.2H_2O$

Molecular weight of Vanadium = 50.9414 g/mol

Molecular weight of Phosphate = 30.97376 g/mol

Molecular weight of Oxygen = 15.9994 g/mol

Molecular weight of Hydrogen = 1.0079 g/mol

Molecular weight of $VOPO_4 \cdot 2H_2O$ = 50.9414 g/mol + (7×15.9994 g/mol) + 30.97376 g/mol + (4×1.0079g/mol)

= 197.94256 g/mol

2. Determine the mol of $VOPO_4 \cdot 2H_2O$ required

No. Of mol of $VOPO_4 \cdot 2H_2O = \frac{mass}{molecular weight}$

$= \frac{10g}{197.94256 g/mol}$

= 0.05052 mol

3. Determine the mol of 1-butanol needed

For 1 mol of $VOPO_4.2H_2O$ mol of 50 mol of 1-butanol is needed.

Thus, for 0.05052 mol of $VOPO_4.2H_2O$ = 0.05052 x 50 mol of 1-butanol

= 2.5260 mol of 1-butanol

4. Determine the volume of 1-butanol used

Molecular formula of 1-butanol = $C_4H_{10}O$

Molecular weight of Carbon = 12.011g/mol

Molecular weight of Oxygen = 15.9994 g/mol

Molecular weight of Hydrogen = 1.0079 g/mol

Molecular weight of $C_4H_{10}O$ = (4×12.011g/mol) + (10×1.0079 g/mol) + 15.9994 g/mol

= 72.1224 g/mol

Density of $C_4H_{10}O$ = 0.802 g/cm^3 at 20ºC

Mass of $C_4H_{10}O$ = 74.1224 g/mol × 2.5260 mol

= 187.2332g

Density = $\frac{Mass}{Volume}$

Volume of 1-butanol = $\frac{Mass}{Density}$

$= \frac{187.2332g}{0.802 g/cm^3}$

= 233.4578 cm^3

APPENDIX C: Dopant Calculations

1. Determine the molecular weight of $VOHPO_4 \cdot 1.5H_2O$

From Periodic Table: H = 1.00794 g/mole V = 50.9415 g/mole
O = 15.9994 g/mole Ba = 137.327 g/mole
P = 30.973763 g/mole Bi = 208.98040 g/mole

Sesquihydrate precursor: $VOHPO_4 \cdot 1.5H_2O$

Molecular weight of Sesquihydrate precursor = [(50.9415) + (15.9994) + (1.00794) + (30.973763) + 4(15.9994) + 1.5[2(1.00794) + (15.9994)]]

= 189.943122 g/mole

2. Determine the mol of $VOHPO_4 \cdot 1.5H_2O$

Dopants are added based on 3.0 g of $VOHPO_4 \cdot 1.5H_2O$ precursor

Thus, for 3.0 g of $VOHPO_4 \cdot 1.5H_2O = \frac{3.0}{189.943122}$

= 0.01579 mole

3. Determine the amounts of dopants needed

For Barium 5 % = 5 % x 0.01579 moles
= 0.0007895 moles
Amount = Molecular weight x 0.0007895 moles
= 261.36 x 0.0007895 moles
= 0.2063 g

For Bismuth 1 % = 1 % x 0.01579 moles
= 0.0001579 moles
Amount = Molecular weight x 0.0001579 moles
= 1461.99 x 0.0001579 moles
= 0.2308 g

For Bismuth 3 % = 3 % x 0.01579 moles
= 0.0004737 mole
Amount = Molecular weight x 0.0004737 moles
= 1461.99 x 0.0004737 moles
= 0.6925 g

For Bismuth 5 % = 3 % x 0.01579 moles
= 0.0007895 moles
Amount = Molecular weight x 0.0007895 moles
= 1461.99 x 0.0007895 moles
= 1.1542 g

Catalyst	Amount of Barium Needed (g)	Amount of Bismuth Needed (g)
Barium 5 %	0.2063	-
Barium 5 %, Bismuth 1 %	0.2063	0.2308
Barium 5 %, Bismuth 3 %	0.2063	0.6925
Barium 5 %, Bismuth 5 %	0.2063	1.1542

APPENDIX D: Crystallite Size Measurement

1. Determine the crystallite size of the catalyst

The crystallite size of the catalyst were calculated using the following formula

Debye-Scherrer Equation: t(Å) $= \frac{0.89\lambda}{\beta_{hkl} \cos \theta_{hkl}}$

Given t = crystallite size for (h k l) plane in unit Angstrom

λ = X-ray wavelength of radiation for CuKα, 1.54 Å

β_{hkl} = Full width at half maximum for the (h k l) plane

Θ_{hkl} = Diffraction angle for the (h k l) plane

Based on the 3 main pyrophosphate peaks at (0 2 0), (2 0 4) and (2 2 1) planes:

VPOs-Ba 5 %

Peak Number	2θ	θ	FWHM (°)	FWHM (rad)
7	22.8400	11.4200	1.1074	0.01933
12	28.4408	14.2204	0.7401	0.01292
13	29.8950	14.9475	0.6100	0.01065

For Peak Number 7: t(Å) $= \frac{0.89\ x\ 1.54}{0.01933\ x \cos(11.4200)}$ **= 72.34 Å**

For Peak Number 12: t(Å) $= \frac{0.89\ x\ 1.54}{0.01292\ x \cos(14.2204)}$ **= 109.44 Å**

For Peak Number 13: t(Å) $= \frac{0.89\ x\ 1.54}{0.01065\ x \cos(14.9475)}$ **= 133.20 Å**

VPOs-Ba 5 %, Bi 1 %

Peak Number	2θ	θ	FWHM (°)	FWHM (rad)
6	22.9200	11.4600	0.9846	0.01718
9	28.3022	14.1511	1.0788	0.01883
10	29.9366	14.9683	0.5845	0.01020

For Peak Number 6: t(Å) $= \frac{0.89\ x\ 1.54}{0.01718\ x\ \cos(11.4600)}$ **= 81.40 Å**

For Peak Number 9: t(Å) $= \frac{0.89\ x\ 1.54}{0.01883\ x\ \cos(14.1511)}$ **= 75.07 Å**

For Peak Number 10: t(Å) $= \frac{0.89\ x\ 1.54}{0.01020\ x\ \cos(14.9683)}$ **= 139.09 Å**

VPOs-Ba 5 %, Bi 3 %

Peak Number	2θ	θ	FWHM (°)	FWHM (rad)
5	22.8800	11.4400	0.9120	0.01592
7	28.3508	14.1754	1.4363	0.02507

For Peak Number 5: t(Å) $= \frac{0.89\ x\ 1.54}{0.01592\ x\ \cos(11.4400)}$ **= 87.84 Å**

For Peak Number 7: t(Å) $= \frac{0.89\ x\ 1.54}{0.02507\ x\ \cos(14.1754)}$ **= 56.39 Å**

VPOs-Ba 5 %, Bi 3 %

Peak Number	2θ	θ	FWHM (°)	FWHM (rad)
5	22.9600	11.4800	0.6328	0.01104
7	28.3716	14.1588	1.4719	0.02569

For Peak Number 5: t(Å) $= \frac{0.89\ x\ 1.54}{0.01104\ x\ \cos(11.4800)}$ **= 126.68 Å**

For Peak Number 7: t(Å) $= \frac{0.89\ x\ 1.54}{0.02569\ x\ \cos(14.1588)}$ **= 55.02 Å**

APPENDIX E: Preparation of Diphenylamine, Ph_2NH Indicator

1. Prepare the indicator

1g of diphenylamine was weighed and dissolved in a few ml of concentrated sulphuric acid, H_2SO_4. Then the solution was transferred to a 100ml volumetric flask and further top up with concentrated H_2SO_4.

APPENDIX F: Preparation of 2M Sulphuric Acid, H_2SO_4 Solution

1. Determine the volume of H_2SO_4 needed

Concentrated H_2SO_4 (95-98 %)

1L = 1.84kg =1840g /1000cm^3 = 1.84g/cm^3

Molecular weight of H_2SO_4 = 2(1.00g/mol) +32.07 g/mol+ 4(16.00 g/mol)

= 98.07 g/mol

Concentration of 95-98 % H_2SO_4= $\frac{1.84 g/cm^3}{98.07 g/mol} \times \frac{95}{100} \times 1000$

= 17.82M

$M_1V_1=M_2V_2$

Where M_1 = concentration of 95-98 % H_2SO_4

M_2= concentration of diluted H_2SO_4 (2m)

V_1= volume of 95-98 % H_2SO_4

V_2= volume of diluted H_2SO_4 (2M)

(17.82M)(V_1) = (2M) (1000cm^3)

V_1 = 112.3 cm^3

APPENDIX G: Preparation of 0.1M Sulphuric Acid , H_2SO_4 Solution

1. Determine the volume of H_2SO_4 needed

$M_1V_1 = M_2V_2$

Where M_1 = concentration of 95-98 % H_2SO_4

M_2 = concentration of diluted H_2SO_4 (0.1m)

V_1 = volume of 95-98 % H_2SO_4

V_2 = volume of diluted H_2SO_4 (0.1M)

$(17.82M)\ (V_1) = (0.1M)\ (1000cm^3)$

$\mathbf{V_1 = 5.61cm^3}$

APPENDIX H: Preparation of 0.01N Potassium Permanganate, $KMnO_4$

1. Determine the weight of $KMnO_4$ in 1000 cm^3 diluted (0.1M) H_2SO_4

Normality, N (eq/L) = M (mol×L) × (*eq*/mol)

$MnO^{4-} + H^+ + 5\ e^- \longleftrightarrow Mn^{2+} + 4H_2O$

$$\text{Molarity, M (mol/L)} = \frac{N(eq/L)}{n(eq/mol)}$$

$$= \frac{0.01}{5}$$

$$= 0.002\ M$$

Molecular Weight of $KMnO_4$ = 39.10 g/mol + 54.94 g/mol + 4(16.00g/mol)

= 158.04g/mol

Weight of $KMnO_4$ in 1000 cm^3 diluted (0.1M) H_2SO_4 = 0.002 ×158.04

= 0.3161g

APPENDIX I: Preparation of 0.01N Ammonium (II) Sulphate, $(NH_4)_2$ Fe $(SO_4)_2.6H_2O$

1. **Determine the weight of $(NH_4)_2$ Fe $(SO_4)_2.6H_2O$ in 1000 cm^3 diluted (0.1M) H_2SO_4**

Normality, N (eq/L) = M (mol×L) × (*eq*/mol)

$Fe^{2+} + e^- \longleftrightarrow Fe^{3+}$

$$\text{Molarity, M (mol/L)} = \frac{N(eq/L)}{n(eq/mol)}$$

$$= \frac{0.01}{1}$$

$$= 0.01 \text{ M}$$

Molecular Weight of $(NH_4)_2$ Fe $(SO_4)_2.6H_2O$ = 2(14.00) g/mol + 20(1.00) g/mol + 55.85g/mol + 2(32.07g/mol) + 14(16.00g/mol)

= 391.99 g/mol

Weight for $(NH_4)_2$ Fe $(SO_4)_2.6H_2O$ in 1000 cm3 diluted (0.1M) H_2SO_4

= 0.00×392.14

= 3.9214g

APPENDIX J: Oxidation State of Vanadium

1. Formulate the average vanadium valence

According to Niwa and Murakami (1982),

$T_1 = V^{4+} + 2V^{3+} = 20\,[MnO^{4-}]\,V_1$ (1)

$T_2 = V^{5+} + V^{4+} + V^{3+} = 20\,[Fe^{2+}]\,V_2$ (2)

$T_3 = V^{5+} = 20\,[Fe^{2+}]\,V_3$ (3)

(2) - (3): $V^{3+} + V^{4+} = 20\,[Fe^{2+}]\,V_2 - 20\,[Fe^{2+}]V_3$ (4)

(1) - (4): $V^{3+} = 20\,[MnO^{4-}]\,V_1 - 20\,[Fe^{2+}]\,V_2 - 20\,[Fe^{2+}]\,V_3$ (5)

Substitute (5) into (1):

$V^{4+} + 2(20\,[MnO^{4-}]\,V_1 - 20\,[Fe^{2+}]\,V_2 + 20\,[Fe^{2+}]\,V_3)$

$= 20\,[MnO^{4-}]\,V_1V^{4+}$

$= 20\,[MnO^{4-}]\,V_1 - 40\,[MnO^{4-}]\,V_1 + 40\,[Fe^{2+}]\,V_2 + 40\,[Fe^{2+}]\,V_3)$

$= 40\,[Fe^{2+}]\,V_2 - 40\,[Fe^{2+}]\,V_3 - 20\,[MnO^{4-}]\,V_1$ (6)

Substitute (5) and (6) into (2):

$20\,[Fe^{2+}]\,V_2 = V^{5+} + (40\,[Fe^{2+}]\,V_2 - 40\,[Fe^{2+}]\,V_3 - 20[MnO^{4-}]\,V_1) + (20\,[MnO^{4-}]\,V_1 - 20\,[Fe^{2+}]\,V_2 + 20\,[Fe^{2+}]\,V_3$

$V^{5+} = 20[Fe^{2+}]\,V_3$ (7)

From (5) V^{3+} $= 20(0.01)\ V_1 - 20(0.01)\ V_3 - 20(0.01)V_1$

$\mathbf{V^{3+} = 0.2(V_1 + V_2 + V_3)}$ **(8)**

From (6) V^{4+} $= 40(0.01)\ V_2 - 40(0.01)\ V_3 - 20(0.01)V_1$

$\mathbf{V^{4+} = 0.4\ V_2 - 0.4\ V_3 - 0.2\ V_1}$ **(9)**

From (7) V^{5+} $= 20\ (0.01)\ V_3$

$\mathbf{V^{5+} = 0.2V_3}$ **(10)**

The average vanadium valence is calculated as:

$$\boldsymbol{V_{AV} = \frac{3V^{3+} + 4V^{4+} + 5V^{5+}}{V^{3+} + V^{4+} + V^{5+}}} \quad \textbf{(11)}$$

2. Determine the average oxidation state

For VPOs-Ba 5 %:

$V_1 = 9.3$ $V_2 = 14.65$ $V_3 = 6.0$

From (9): V^{4+} $= 0.4\ V_2 - 0.4\ V_3 - 0.2\ V_1$

$= 0.4\ (14.65) - 0.4\ (6.0) - 0.2\ (9.3)$

$= 1.6$

From (10): V^{5+} $= 0.2\ V_3$

$= 0.2(6.0)$

$= 1.2$

From (11): $V_{AV} = \frac{3(0)+4(1.6)+5(1.2)}{0+1.6+1.2}$

= 4.4286

For VPOs-Ba 5 %, Bi 1 %:

$V_1 = 8.25$ $V_2 = 13.45$ $V_3 = 7.0$

From (9): $V^{4+} = 0.4\ V_2 - 0.4\ V_3 - 0.2\ V_1$

$= 0.4\ (13.45) - 0.4\ (7.0) - 0.2\ (8.25)$

$= 1.6$

From (10): $V^{5+} = 0.2\ V_3$

$= 0.2(7.0)$

$= 1.2$

From (11): $V_{AV} = \frac{3(0)+4(13.45)+5(8.25)}{0+13.45+8.25}$

= 4.6008

For VPOs-Ba 5 %, Bi 3 %:

$V_1 = 5.0$ $V_2 = 11.25$ $V_3 = 6.9$

From (9): $V^{4+} = 0.4\ V_2 - 0.4\ V_3 - 0.2\ V_1$

$= 0.4\ (11.25) - 0.4\ (6.9) - 0.2\ (5.0)$

$= 1.6$

From (10): $V^{5+} = 0.2\ V_3$

$= 0.2(6.9)$

$= 1.2$

From (11): $V_{AV} = \frac{3(0)+4(11.25)+5(5.0)}{0+11.25+5.0}$

= 4.6509

For VPOs-Ba 5 %, Bi 5 %:

$V_1 = 3.2$ $V_2 = 10.6$ $V_3 = 7.4$

From (9): $V^{4+} = 0.4\ V_2 - 0.4\ V_3 - 0.2\ V_1$

$= 0.4\ (10.6) - 0.4\ (7.4) - 0.2\ (3.2)$

$= 1.6$

From (10): $V^{5+} = 0.2\ V_3$

$= 0.2(3.2)$

$= 1.2$

From (11): $V_{AV} = \frac{3(0)+4(10.6)+5(3.2)}{0+10.6+3.2}$

= 4.6980

APPENDIX K: TPR Analysis

1. Determine the Reduction activation energy, E_r

Required formulas:

$E_a = T_m \times 0.066$ where T_m : maximum temperature

$\chi = Ae^{\left(\frac{-E_a}{R\ x\ T_m}\right)}$ where A : 1×10^{13}

R : 0.001987 kcal K^{-1} mol^{-1}

$[H_2] = \frac{P}{R\ x\ T}$ where P : Pressure in atm

T : Ambient temperature, 298 K

R : 82.056 cm^3 atm K^{-1} mol^{-1}

$E_r = RT_m In\left[\frac{A(H_2)}{\chi}\right]$ where R : 0.001987 kcal K^{-1} mol^{-1}

The values for $\chi = 0.03754\ s^{-1}$ and $[H_2] = 4.036 \times 10^{-7}$ mol cm^3

For VPOs-Ba 5 %

Peak 1: $E_r = RT_m In\left[\frac{A(H_2)}{\chi}\right]$

$= (0.001987)(805)\ In\left[\frac{(1x10^{13})(4.306x10^{-7})}{0.03754}\right]$

$= 29.5804$ kcal $mol^{-1} \times 4.184 \frac{J}{cal}$

$= 123.7644$ KJ mol^{-1}

Peak 2: $E_r = RT_m In\left[\frac{A(H_2)}{\chi}\right]$

$= (0.001987)(885)\ In\left[\frac{(1x10^{13})(4.306x10^{-7})}{0.03754}\right]$

$= 32.5200$ kcal $mol^{-1} \times 4.184 \frac{J}{cal}$

$= 136.2768$ KJ mol^{-1}

Peak 3: $E_r = RT_m In\left[\frac{A(H_2)}{\chi}\right]$

$= (0.001987)(1062)\ In\left[\frac{(1x10^{13})(4.306x10^{-7})}{0.03754}\right]$

$= 39.0241$ kcal $mol^{-1} \times 4.184 \frac{J}{cal}$

$= 163.2768$ KJ mol^{-1}

For VPOs-Ba 5 %, Bi 1 %

Peak 1: $E_r = RT_m In\left[\frac{A(H_2)}{\chi}\right]$

$= (0.001987)(794)\ In\left[\frac{(1x10^{13})(4.306x10^{-7})}{0.03754}\right]$

$= 29.176$ kcal $mol^{-1} \times 4.184 \frac{J}{cal}$

$= 122.073$ KJ mol^{-1}

Peak 2: $E_r = RT_m In\left[\frac{A(H_2)}{\chi}\right]$

$= (0.001987)(888)\ In\left[\frac{(1x10^{13})(4.306x10^{-7})}{0.03754}\right]$

$= 32.6303$ kcal mol^{-1} x $4.184\ \frac{J}{cal}$

= 136.5252 KJ mol^{-1}

Peak 3: $E_r = RT_m In\left[\frac{A(H_2)}{\chi}\right]$

$= (0.001987)(913)\ In\left[\frac{(1x10^{13})(4.306x10^{-7})}{0.03754}\right]$

$= 33.5482$ kcal mol^{-1} x $4.184\ \frac{J}{cal}$

= 140.3657 KJ mol^{-1}

For VPOs-Ba 5 %, Bi 3 %

Peak 1: $E_r = RT_m In\left[\frac{A(H_2)}{\chi}\right]$

$= (0.001987)(858)\ In\left[\frac{(1x10^{13})(4.306x10^{-7})}{0.03754}\right]$

$= 31.6384$ kcal mol^{-1} x $4.184\ \frac{J}{cal}$

= 132.375 KJ mol^{-1}

Peak 2: $E_r = RT_m In\left[\frac{A(H_2)}{\chi}\right]$

$= (0.001987)(895)\ In\left[\frac{(1x10^{13})(4.306x10^{-7})}{0.03754}\right]$

$= 32.8875$ kcal mol^{-1} x $4.184\ \frac{J}{cal}$

= 137.6013 KJ mol^{-1}

Peak 3: $E_r = RT_m In\left[\frac{A(H_2)}{\chi}\right]$

$= (0.001987)(918)\ In\left[\frac{(1x10^{13})(4.306x10^{-7})}{0.03754}\right]$

$= 33.7327$ kcal mol^{-1} x $4.184\ \frac{J}{cal}$

= 141.1376 KJ mol^{-1}

For VPOs-Ba 5 %, Bi 5 %

Peak 1: $E_r = RT_m In\left[\frac{A(H_2)}{\chi}\right]$

$= (0.001987)(831)\ In\left[\frac{(1x10^{13})(4.306x10^{-7})}{0.03754}\right]$

$= 30.6427$ kcal mol^{-1} x $4.184\ \frac{J}{cal}$

= 128.209 KJ mol^{-1}

Peak 2: $E_r = RT_m In\left[\frac{A(H_2)}{\chi}\right]$

$= (0.001987)(887)\ In\left[\frac{(1x10^{13})(4.306x10^{-7})}{0.03754}\right]$

$= 32.5935$ kcal mol^{-1} x $4.184\ \frac{J}{cal}$

= 136.3712 KJ mol^{-1}

Peak 3: $E_r = RT_m In\left[\frac{A(H_2)}{\chi}\right]$

$= (0.001987)(906)\ In\left[\frac{(1x10^{13})(4.306x10^{-7})}{0.03754}\right]$

$= 33.2917$ kcal mol^{-1} x $4.184\ \frac{J}{cal}$

= 139.2925 KJ mol^{-1}

2. Determine the amount of oxygen removed

For VPOs-Ba 5 %

Peak 1: 79.57145 μmolg^{-1} **= 7.957 x 10^{-5} mol g^{-1}**

= (7.957 x 10^{-5}) x (6.02 x 10^{23})

= 4.790 x 10^{19} atom g^{-1}

Peak 2: 361.77215 μmolg^{-1} **= 3.618 x 10^{-4} mol g^{-1}**

= (3.618 x 10^{-4}) x (6.02 x 10^{23})

= 2.178 x 10^{20} atom g^{-1}

Peak 3: 927.89605 μmolg^{-1} **= 9.276 x 10^{-4} mol g^{-1}**

= (9.276 x 10^{-4}) x (6.02 x 10^{23})

= 5.584 x 10^{20} atom g^{-1}

For VPOs-Ba 5 %, Bi 1 %

Peak 1: 1870.1241 μmolg^{-1} **= 1.870 x 10^{-3} mol g^{-1}**

= (1.870 x 10^{-3}) x (6.02 x 10^{23})

= 1.126 x 10^{21} atom g^{-1}

Peak 2: 2328.1468 μmolg^{-1} **= 2.328x 10^{-3} mol g^{-1}**

= (2.328 x 10^{-3}) x (6.02 x 10^{23})

= 1.401 x 10^{21} atom g^{-1}

Peak 3: 3606.4423 μmolg^{-1} **= 3.606 x 10^{-3} mol g^{-1}**

= (3.606 x 10^{-3}) x (6.02 x 10^{23})

= 2.171x 10^{21} atom g^{-1}

For VPOs-Ba 5 %, Bi 3 %

Peak 1: 672.4155 $\mu molg^{-1}$ **= 6.722 x 10^{-4} mol g^{-1}**

= (6.722 x 10^{-4}) x (6.02 x 10^{23})

= 4.047 x 10^{20} atom g^{-1}

Peak 2: 2105.3684 $\mu molg^{-1}$ **= 2.105 x 10^{-3} mol g^{-1}**

= (2.105 x 10^{-3}) x (6.02 x 10^{23})

= 1.268 x 10^{21} atom g^{-1}

Peak 3: 2291.2589 $\mu molg^{-1}$ **= 2.291x 10^{-3} mol g^{-1}**

= (2.291 x 10^{-3}) x (6.02 x 10^{23})

= 1.379 x 10^{21} atom g^{-1}

For VPOs-Ba 5 %, Bi 5 %

Peak 1: 1899.3883 $\mu molg^{-1}$ **= 1.899 x 10^{-3} mol g^{-1}**

= (1.899 x 10^{-3}) x (6.02 x 10^{23})

= 1.143 x 10^{21} atom g^{-1}

Peak 2: 2466.0918 $\mu molg^{-1}$ **= 2.466 x 10^{-3} mol g^{-1}**

= (2.466 x 10^{-3}) x (6.02 x 10^{23})

= 1.485 x 10^{21} atom g^{-1}

Peak 3: 3252.4577 $\mu molg^{-1}$ **= 3.252 x 10^{-3} mol g^{-1}**

= (3.252 x 10^{-3}) x (6.02 x 10^{23})

= 1.958 x 10^{21} atom g^{-1}

3. Determine the ratio of oxygen removed

The first and second peaks belong to V^{5+} and the last peak belongs to V^{4+}.

Sum of Peak 1 and peak 2 = Total V^{5+}

Sum of Peak 3 = Total V^{4+}

For VPOs-Ba 5%

Total V^{5+} $= (4.790 \times 10^{19}) + (2.178 \times 10^{20})$

$= 2.65682 \times 10^{20}$ atom g^{-1}

Total V^{4+} $= 5.584 \times 10^{20}$ atom g^{-1}

Ratio of V^{5+}/ V^{4+} $= \frac{2.65682 \times 10^{20}}{5.584 \times 10^{20}}$

= 0.476

Ratio of V^{4+}/ V^{5+} $= \frac{5.584 \times 10^{20}}{2.65682 \times 10^{20}}$

= 2.101

For VPOs-Ba 5 %, Bi 1 %

Total V^{5+} $= (1.126 \times 10^{21}) + (1.401 \times 10^{21})$

$= 2.527 \times 10^{21}$ atom g^{-1}

Total V^{4+} $= 2.171 \times 10^{21}$ atom g^{-1}

Ratio of V^{5+}/ V^{4+} $= \frac{2.527 \times 10^{21}}{2.171 \times 10^{21}}$

= 1.164

Ratio of V^{4+}/ V^{5+} $= \frac{2.171 \times 10^{21}}{2.527 \times 10^{21}}$

= 0.859

For VPOs-Ba 5 %, Bi 3 %

Total V^{5+} $= (4.047 \times 10^{20}) + (1.268 \times 10^{21})$

$= 1.6727 \times 10^{21}$ atom g^{-1}

Total V^{4+} $= 1.379 \times 10^{21}$ atom g^{-1}

Ratio of V^{5+}/ V^{4+} $= \frac{1.6727 \times 10^{21}}{1.379 \times 10^{21}}$

= 1.212

Ratio of V^{4+}/ V^{5+} $= \frac{1.379 \times 10^{21}}{1.6727 \times 10^{21}}$

= 0.825

For VPOs-Ba 5 %, Bi 5 %

Total V^{5+} $= (\mathbf{1.143 \times 10^{21}}) + (\mathbf{1.485 \times 10^{21}})$

$= 2.628 \times 10^{21}$ atom g^{-1}

Total V^{4+} $= \mathbf{1.958 \times 10^{21}}$ atom g^{-1}

Ratio of V^{5+}/ V^{4+} $= \frac{2.628 \times 10^{21}}{1.958 \times 10^{21}}$

= 1.342

Ratio of V^{4+}/ V^{5+} $= \frac{1.958 \times 10^{21}}{2.628 \times 10^{21}}$

= 0.745